SITE EFFECTS "ON THE ROCK": THE CASE OF CASTELVECCHIO SUBEQUO (L'AQUILA, CENTRAL ITALY)

Marzorati S.[1], Ladina C.[1], Falcucci E.[2], Gori S.[2], Saroli M.[3], Ameri G.[4], Galadini F.[2]

[1] Istituto Nazionale di Geofisica e Vulcanologia, Centro Nazionale Terremoti

[2] Istituto Nazionale di Geofisica e Vulcanologia, Sezione di Roma1

[3] Dipartimento di Meccanica, Strutture, Ambiente e Territorio, Università di Cassino

[4] Istituto Nazionale di Geofisica e Vulcanologia, Sezione di Milano-Pavia

Corresponding author: Simone Marzorati, Istituto Nazionale di Geofisica e Vulcanologia, Centro Nazionale Terremoti, Sede di Ancona, Strada Cameranense 1, 60131 Passo Varano (AN), Italy, email: simone.marzorati@ingv.it

Abstract

The April 6, 2009 L'Aquila earthquake was responsible for an "anomalous", relatively high degree of damage (i.e. Is 7 MCS scale) at Castelvecchio Subequo (CS). Indeed, the village is located at source-to-site distance of about 40 km, and it is surrounded by other inhabited centres to which considerably lower intensities, i.e. Is 5-6, have been attributed. Moreover, the damage was irregularly distributed within CS, being mainly concentrated in the uppermost portion of the old village. Geophysical investigations (ambient seismic noise and weak ground motions analyses) revealed that site effects occurred at CS. Amplifications of the ground motion, mainly striking NE-SW, have been detected at the uppermost portion of the carbonate ridge on which the village is built. Geological/structural and geomechanical field surveys defined that the CS ridge is affected by sets of fractures, joints and shear planes – mainly roughly NW-SE and N-S trending – that are related to the deformation zone of the Subequana valley fault system and to transfer faults linking northward the mentioned tectonic feature with the Middle Aterno Valley fault system. In particular, our investigations highlight that seismic amplifications occur where joints set NW-SE trending are open. On the other hand, no amplification is seen in portions of the ridge where the bedrock is densely fractured but no open joints occur. The fracture opening seems related to the toppling tendency of the bedrock slabs, owing to the local geomorphic setting. These investigations suggest that the detected amplification of the ground motion is probably related to the polarization of the seismic waves along the Castelvecchio Subequo ridge, with the consequent oscillation of the rock slabs perpendicularly to the fractures azimuth.

Keywords

Site effects; rock sites; spectral ratios; ambient seismic noise; structural characteristics; jointing conditions; geomechanical analysis; 2009 L'Aquila earthquake; central Italy.

1. Introduction

On April 6, 2009 the central Apennines have been struck by a Mw 6.3 earthquake, the largest in Italy since Irpinia 1980. The seismic event has been caused by the activation of an about 10-13-km-long (at surface) extensional tectonic structure, i.e. the Paganica fault (hereafter PF), located about 10 kilometres E of the city of L'Aquila (e.g. Falcucci et al. 2009; Emergeo Working Group 2010; Boncio et al. 2010).

The quake severely damaged the densely populated L'Aquila plain area and surroundings, causing 308 fatalities and widespread destruction in L'Aquila and in tens of villages (e.g. Onna, Paganica, San Demetrio ne' Vestini, Fossa, etc.).

The macroseismic survey, performed in the aftermath of the seismic event, defined the intensities (MCS scale) of the 2009 earthquake (Galli and Camassi 2009): the mesoseismal area (i.e. Is>7-8), elongated roughly 20 km SE of the epicentral zone along the Aterno river valley, comprised 16 villages with Is≥8, six of which suffered damage estimated with Is≥9. The maximum intensities, i.e. Imax 9-10, were attributed to the villages of Castelnuovo and Onna (Fig. 1a).

As expected, the damage decreased moving away from the source. In particular, along the Aterno river valley, the intensities decreased to Is=5-6 about 40 km far from L'Aquila. Nevertheless, the intensity distribution revealed an evident "anomaly" in the southern portion of the damaged region, i.e. in the Subequana valley: here, Is=7, 6-7 and 7 were indeed attributed to three villages, namely Castelvecchio Subequo, Castel di Ieri and Goriano Sicoli, respectively, located among others that were affected by evidently lower damage, i.e. estimated with Is=5-6 (such as Molina Aterno, Goriano Valli and Acciano) and 6 (such as Secinaro) (Fig. 1a, inset).

In particular, besides the anomalous intensity, Castelvecchio Subequo (hereafter CS) showed a peculiar distribution of damage. The strongest damage affected, indeed, the uppermost portion of the village, where the partial collapse of several buildings occurred. Although the aging and the characteristics of the buildings have certainly contributed to the intensity related to the 2009 seismic event, nevertheless the oldest portion of the village has not been affected by a homogeneous damage degree.

In light of this, the present work analyses the CS case, aiming at unveiling the possible cause of the "anomalous" MCS intensity (considering the distance from the causative fault of the earthquake) and the irregular distribution of the damage within the village.

More specifically, we will evaluate the possible occurrence of site effects along the narrow carbonate ridge on which the village is built by means of ambient seismic noise and weak ground motions analyses. These geophysical investigations will be coupled with detailed geologic/structural field observations performed in the area of CS as well as with quantitative geomechanical characterisation of the rock mass. Our aim is to define the role played by the local geologic characteristics and complexities in the local seismic response.

Within this light, it must be noted that several studies pointed out the occurrence of seismic amplifications along topographic "irregularities" (Bard, 1982; Çelebi 1987; Kawase and Aki 1990; Ponti and Wells 1991; Pedersen et al. 1994; Chavez-Garcia et al. 1996; Spudich et al. 1996; Athanasopoulos et al. 1999; Faccioli et al. 2002; Massa et al. 2010; Pischiutta et al. 2010). In particular, the geometrical features of morphological

conditions are used in many works to simulate the amplification on hills and crests (Boore, 1972; Griffiths and Bollinger, 1979; Sánchez-Sesma et al., 1982; Bard and Tucker, 1985; Sánchez-Sesma, 1985;Géli and Bard, 1988; Sánchez-Sesma, 1990; Sánchez-Sesma and Campillo, 1991; Chávez-García et al., 1996; Bouchon and Barker, 1996; Komatitsch and Vilotte, 1998; Le Brun et al., 1999; Paolucci, 2002) although, in many cases, the simulations underestimate the amplifications, as the overall heterogeneities of the sites are not supported by the resolutions of the models. In other case studies, the surface weathering (Le Brun et al. 1999; Graizer 2009), in any cases due to presence of faults (Rovelli et al. 2002), and the jointing conditions of the rock masses (Martino et al., 2006; Hailemikael et al., 2010) are invoked to explain seismic amplification.

The results of the present work – derived from the necessary merger of geological and geophysical investigations – are of practical importance as they constrain the guidelines for reconstruction and repairs of the historical buildings in a typical picturesque village of the central Apennine region.

2. Geological setting

2.1 Seismotectonic framework of the central Apennines

The Apennine belt formed since the Oligocene, during the Alpine-Himalayan orogenesis. The "backbone" of the chain is represented by thrust and fold systems that progressively migrated towards E and NE, displacing Meso-Cenozoic limestone sequences (e.g. Patacca et al. 2008).

Since the Pliocene, extensional deformation affected the central Apennines and displaced the structures inherited by the compressive tectonics (e.g. Cavinato and De Celles 1999). This "new" tectonic phase resulted in NW-SE trending normal fault systems, paralleling the axis of the chain. The activity of these structures through the Quaternary determined the formation of several intermontane depressions, such as the Fucino, L'Aquila, Sulmona, Rieti, Norcia and Subequana basins (the last is the area where the present study has been performed) (e.g. Galadini and Messina 2004). Most of these depressions – basically half-graben structures bordered on the eastern flanks by normal faults – hosted a continental deposition since the Pliocene.

Extensional deformation in the central Apennines is presently active, as witnessed by i) geological evidence of Late Pleistocene-Holocene activity along NW-SE trending normal fault systems (Fig. 1b) (e.g. Galadini and Galli 2000; Boncio et al. 2004); ii) geodetic (GPS) data, indicating an extension rate of about 3 mm/yr across the chain (Devoti et al. 2008); and iii) instrumental seismicity data, which have identified earthquake focal mechanisms consistent with NW-SE normal ruptures (e.g. Pondrelli et al. 2006; Bagh et al. 2007).

The active normal faults of the central Apennines are considered as the expression at the surface of seismogenic sources, potentially responsible for earthquakes with magnitude up to 6.5-7. Some of these faults activated in historical times, causing strong seismic events, such as the 1349 (Mw 6.6), 1703 (Jan. 14; Mw 6.7), 1703 (Feb. 2; Mw 6.7) and 1915 (Mw 7.0) events (Working Group CPTI, 2008) (Fig. 1b). In particular, the April 6, 2009 earthquake occurred in a sector of the central Apennines that has been already struck by several moderate-to-large magnitude earthquakes in the past, as the 9 September 1349 (Mw 6.5), 2

February 1703 (Mw 6.7), 1461 (Mw 6.4), 1762 (Mw 5.9), 1916 (Mw 5.2) and 1958 (Mw 5.2) (Rossi et al. 2005; Working Group CPTI 2008; Tertulliani et al. 2009).

As for the 2009 seismic event, geological and geophysical investigations agreed in defining the mentioned PF as the causative fault of the earthquake. Indeed, field evidence of coseismic surface ruptures along the tectonic structure – detected between the villages of Collebrincioni and San Gregorio – matched with the intersection with the surface of the fault modelled by means of GPS (e.g. Anzidei et al. 2009) and InSAR coseismic data (e.g. Atzori et al. 2009).

2.2. The Subequana valley

The village of Castelvecchio Subequo is located about 40-50 km SE of L'Aquila, along the eastern flank of the mentioned Subequana valley, an intermontane tectonic basin adjacent to the Aterno river valley.

The Quaternary evolution of the Subequana depression has been influenced by the activity of a normal fault system that borders the eastern side of the basin (Miccadei et al. 1997; Calamita et al. 2000; Falcucci et al. in press), i.e. the Subequana valley normal fault system (hereafter SVF) (Fig. 1c). This tectonic element affects the SW slopes of Mt. Urano, an anticline structure related to a NE-verging thrust that displaced Meso-Cenozoic limestone and marls sequences pertaining to different paleogeographic domains (e.g. Miccadei et al. 1997; Foglio CARG 2009). The Quaternary SVF activity led to the formation of a sedimentary trap, i.e. the Subequana basin, where a 200-300-m-thick continental sequences deposited (e.g. Bosi and Bertini 1970; Falcucci et al. 2009).

In detail, the SVF is made of two main parallel segments: an easternmost segment, detectable at the intermediate-upper sectors of the slopes and a westernmost branch, affecting the base of Mt. Urano (Falcucci et al. in press). The latter, in turn, is made of at least three sub-segments having a dextral en-echelon arrangement (Fig. 1c).

The activity of the SVF during the Late Quaternary is testified by the displacement of Late Holocene deposits along the westernmost strand of the fault system, detected by means of geological field investigations and paleoseismological trenching (Falcucci et al. in press).

3. Geological/structural and geomechanical investigations at Castelvecchio Subequo

Castelvecchio Subequo raises at about 500 m a.s.l. on a small NW-SE elongated carbonate ridge, located at the northern termination of Mt. Urano and bounded towards E and W by stream incisions, up to 20-30 m deep. The eastern incision morphologically separates the ridge from the Mt. Urano SW slopes (Fig. 1d).

At the southern portion of the CS ridge, Cretacic limestone – pertaining to the Maiolica Formation – crop out (Foglio CARG 2009), while the northern portion is made of fluvio-lacustrine sediments, Lower-Middle Pleistocene in age (Foglio CARG 2009), unconformably overlaying limestone sequences of the Maiolica and Scaglia Detritica Formations (Foglio CARG, 2009) (Fig. 2).

Field observations indicate that the area of the old village is characterised by a complex structural setting. Indeed, the ridge is located at the northern termination of the SVF westernmost branch. Here, the fault splits

into two splays (Fig. 2), bounding the ridge to NE and to SW (Falcucci et al. in press).

As visible along the northern sector of the village, the eastern splay places in contact the carbonate substratum, outcropping in the footwall, with the previously mentioned Early-Middle Pleistocene fluvio-lacustrine sequence, exposed in the hanging wall.

Moreover, within the area of CS, the westernmost SVF splay intersects further tectonic elements, about N-S and NNE-SSW trending, characterised by a normal-to-transtensive kinematics (Fig. 2). In particular, according to Falcucci et al. (in press), these structural features, responsible for the displacement of fluvial deposits of probable Late Pleistocene age, represent transfer faults that structurally and kinematically link the SVF with a further active tectonic structure, namely the Middle Aterno Valley normal fault (e.g. Galadini and Galli 2000).

As depicted below, such complex active fault pattern has strongly influenced – and it is still influencing – the structural characteristics of the carbonate rock mass on which CS is founded, determining the present structural setting of the ridge.

The activity of the westernmost SVF branch and of the mentioned transfer faults determined pervasive brittle deformation on the rock masses, overprinted on structural features inherited by the compressive tectonic phase. Here, indeed, transpressive-to-reverse shear planes, probably related to a back-thrust outcropping at the base of the Mt. Urano slopes, have been cross-cut by shear planes related to the SVF strand (Fig. 3).

The deformation related to the faults resulted in sets of fractures, conjugate shear planes – paralleling the SVF branch and the transfer faults – that have heavily modified the primary fabric of the limestone, almost completely obliterating the original bedrock stratification (Fig. 4a).

In particular, in the southernmost sector of the CS ridge, the bedrock exposed at the lowermost portion of the small relief is affected by near vertical, narrowly spaced shear planes and closed fractures (Fig. 4b, 2).

In the uppermost portion of the ridge, instead, the rock mass is affected by opening mode discontinuities (Fig. 4c), i.e. open, planar parallel fractures and joints, that separate different slabs of limestone bedrock. In detail, at the uppermost sectors, these fractures *i*) have irregular spacing that ranges from tens of centimetres, along the eastern flank of the ridge, to some metres, along the western side; *ii*) are up-to-several-tens-of-cm wide (the width decreases with depth); *iii*) are mainly NW-SE trending, i.e. strike parallel to the SVF segment; and *iv*) display opposite dip direction, i.e. towards W and E along the eastern and western flanks of the ridge, respectively (Fig. 4d, e, f).

Our observations indicate that the fractures originated from antithetic and synthetic shear planes mainly related to the SVF segment and, secondarily, to the above mentioned transfer faults (Fig. 4f). The progressive spreading of the fractures is probably due to the tendency of the rock blocks to topple towards the incisions bounding the CS ridge.

In order to achieve a quantitative picture of the above described structural characteristics of the rock mass – in particular of the jointing condition of the ridge – we performed a geomechanical analysis along 10 geomechanical stations corresponding to bedrock outcrops 1-to-4-m^2 wide (Fig. 2).

We proceeded with two steps: firstly, we defined the main discontinuities sets, i.e. structural features having

homogeneous geometrical features; secondly, we performed a detailed characterisation of each set. This allowed the definition of conventional geomechanical indexes, namely Jv (number of discontinuities per unit volume), JRC (Joint Roughness Coefficient), Undulation, RQD (Rock Quality Designation) (ISRM 1978; Hudson and Priest 1979; Hoek and Bray 1981) (Table 1).

The distinction of the jointing sets has been performed by adopting a subjective criterion (ISRM 1978), taking into account those structural features which mainly influence the mechanical characteristics of the rock mass. The heavy urbanisation of the area prevented the possibility to adopt an objective criterion due to the lack an homogeneous distribution of significant bedrock outcrops.

The collected data revealed a very good correlation between the different sets of joints and the main tectonic features affecting the CS ridge, i.e. the above mentioned SVF western segment and the transfer faults. In detail, we distinguished four prevailing joint domains – two mainly N-S–to–NNE-SSW trending and two oriented roughly NW-SE–to–NNW-SSE – having different morphological characteristics and geomechanical properties. Each system is here expressed with its azimuth and dip: I) N10/80, II) N15/75, III) N160/70 and IV) N140/75 (Table 1).

These analyses allowed to confirm the difference in the deformation style between the lowermost and the uppermost portions of the ridge, as already defined by the qualitative structural observations. Indeed, as shown by the data collected in the different geomechanical stations analysed along the ridge, the bedrock of the lowermost sectors of the rock mass is characterised by poorer geomechanical characteristics – as suggested by the Jv and RQD indexes – (e.g. stations CS3, CS4, CS6, Table 1) than that exposed at the uppermost part of the ridge where, as exposed above, open fractures have been identified (e.g. stations CS5 and CS8, Table 1). The influence that these data have in terms of evaluation of the local seismic response will be analysed in the discussion.

4. Geophysical survey

Campaigns of ambient seismic noise recording were carried out between July, 2009 and February, 2010 with the aim of obtaining information about possible local amplification of the ground motion in the area of CS.

We have acquired twenty-two reliable ambient seismic noise recordings along the CS ridge (from the basal portion to the uppermost sector), in the ancient portion of the village and in the surrounding areas (Table 2, Figs .5).

Microtremors were recorded through two portable seismic stations equipped with Lennartz 5s (www.lennartz-electronic.de) velocimetric sensors and 24-bit Reftek 130 (www.reftek.com) Digital Acquisition Systems (hereafter DAS).

The ambient seismic noise measurements were carried out on exposures of limestone bedrock detected within the village and on pavings superposed to the bedrock. All the measurements were performed in free-field, courtyards, squares and cellars excavated in the bedrock (Table 2; Fig. 6).

Besides, a small temporary seismic network (made of three seismic stations) was installed from September 17 to November 4, 2009 to collect earthquake waveforms. The stations were equipped with Episensor FBA

accelerometers (www.kinemetrics.com), in addition to velocimetric sensor Lennartz 5s., in order to avoid the saturation of digital seismic signals due to strong ground motions. The Reftek 130 DAS recorded a continuous dataset with rate of 100 samples per second (hereafter sps).

The geometry of the temporary seismic network, shown in Figures 5 and 7, has been defined basing on 1) geologic observations, that highlighted the different degree of fracturing of the CS ridge and the Mt. Urano SW slope, and 2) on the ambient seismic noise campaigns which, as depicted in the following paragraph, showed no ground motion amplification along the Mt. Urano SW slopes and different amplification values between the base and the uppermost portion of the CS ridge.

4.1 Ambient seismic noise: data processing and spectral ratio analysis

The ambient seismic noise recordings were manually selected in order to remove the possible traces of signal affected by disturbances and artificial transients. Each measure lasted at least 30 minutes, with rate of 100 sps. Also, the mean, the linear trend and the instrumental response were removed from all the recordings. The waveforms were windowed in 120-seconds-long time series. Each trace was rotated between 0° and 175° (with steps of 5°) to investigate preferential directions of the amplifications. Then, a band-pass Butterworth 4 poles filter between 0.2 and 25 Hz and a cosine taper 10% were applied to every window. The Power Spectral Density (hereafter PSD) was calculated for the East-West (hereafter EW), North-South (hereafter NS) and vertical (hereafter VT) components, as described in McNamara and Buland (2004); the single PSD was smoothed using the Konno and Ohmachi (1998) technique (with smoothing parameter, b=40). In order to compute the Horizontal to Vertical Spectral Ratio (Nogoshi and Igarashi, 1971; Nakamura, 1989) from the ambient noise recordings (hereafter NHVSR) for each considered azimuth, the ratio between the spectrum of the radial and vertical components was calculated. The resulting NHVSR was obtained by geometrical mean of the NHVSRs from all the selected signal windows.

In Figures 8 and 9, we present the results of the NHVSR in terms of amplification curves and polar diagrams (i.e., amplitude-frequency-azimuth plots). Furthermore, Table 2 shows the synoptic description of the measurement sites and the values of the NHVSR main parameters.

The measurements CVS4, CVS6, CVS7, CV26, CV30, performed along the western flank of the ridge (sector WF), show moderate amplifications between 1 and 8 Hz (Fig. 10 WF). In particular, CV26 and CV30 sites, located at the base of the ridge, provided NHVSR slightly larger than 2. Moreover, it is worthy of note that these NHVSR are heterogeneous as regards the frequency of the peaks and the direction of the amplification at each site (Fig. 9).

As for the measurements performed along the eastern flank (sector EF), the NHVSR show site amplifications with amplitudes smaller than 6 (Fig. 8 EF). The CVS1, CV16, CVS2 stations show neither evident single peaks nor a preferential direction of amplification (Fig. 9).

Figure 8 UPR, instead, points out strong amplification of ground motion of the horizontal components compared to that of the vertical components derived from the measurements performed at the uppermost portion of the ridge (sector UPR). The site amplifications appear in the frequency range 1.5-8 Hz, with larger

amplitudes around 3-4 Hz. The direction of the maximum amplifications is about 70°-250° striking, i.e. perpendicular to the main axis of the ridge elongation. In particular, the NHVSR of CV40 and CV85 (Fig. 8 UPR) show amplifications in directions that are different from those of the other measurement of the UPR sector (Fig. 9).

Finally, the measurements performed in the surrounding areas of CS (CVS9, CV72, CV86) and along Mt. Urano (CV18) (sector SA) provide NHVSR that displays no site amplification, (sector SA in Fig. 8). On this basis, the Mt. Urano flank has been chosen as reference site and a seismic station was installed for the temporary network (CA02 in Fig. 5).

4.2 Earthquake data: processing and spectral ratio analysis

A dataset of earthquake waveforms was created selecting the events from the Italian Seismological Instrumental and Parametric Data-basE (ISIDE, http://iside.rm.ingv.it). The earthquakes were selected within an area of 100 km from CS, from September 17 to November 4, 2009 . We selected 903 events with magnitudes (Ml) comprised between 0.1 and 4.1 (Fig. 10). Some of these seismic events were localized in the L'Aquila and Cassino areas, NE and S of the Subequana valley, respectively.

We followed the following procedure: firstly, we performed manual picking of the S-phase on the horizontal components and events with a low signal-to-noise ratio were removed. Then, we checked that no saturation of the seismic signal occurred in the velocimetric traces.

This procedure resulted in 295, 234 and 308 events, recorded by CA01, CA02 and CA03 stations, respectively.

The off-set, the linear trend and the instrumental response were removed from each waveform. The Horizontal to Vertical Spectral Ratio (hereafter HVSR) (Lermo and Chavez-Garcia 1993) and Standard Spectral Ratio (hereafter SSR) (Borcherdt 1970) analyses were applied to the selected dataset with the aim of obtaining an estimate of local seismic response. The spectral ratios were calculated on time-windows of 10 seconds from the onset of the S phase. A band-pass Butterworth filter with 4 poles between 0.2-25 Hz and a 10% cosine tapering were applied. Then, the FFT of the signal window was calculated and smoothed with Konno-Ohmachi technique (as done for the NHVSR).

The NS and EW spectra were divided by the vertical spectrum for each seismic event in order to obtain a collection of HVSR. Similarly, the horizontal and vertical spectra of CA03 were divided by the horizontal and vertical spectra of CA02 and CA01, respectively, to obtain a collection of SSR. Moreover, the spectra of CA01 was divided by the spectra of CA02. Finally, a geometric mean of all events spectral ratios was considered to obtain HVSR and SSR at each site.

The results obtained from the HVSR analysis are here described: as for the reference station (CA02), HVSR has a flat trend (Fig.11 bottom). This can be attributed to the fact that the station has been installed at the lowermost portion of Mt. Urano ridge where no significant amplification (e.g. due to topographic effect) are expected. On the contrary, the HVSR of the stations at the base (CA01) and at the top (CA03) of the ridge show significant amplifications. In both cases, the larger amplification occur on the EW component (Figs. 11

middle and 11 top, respectively). In detail, at CA01 station, the EW component is amplified in the frequency range 5-8 Hz with respect to the vertical component while, HVSR of CA03 station is greater than 2 between 1 and 8 Hz, and the maximum amplification appears around 3 Hz.

SSRs are calculated for the three components of the signal (Fig.12). The station CA03 was compared with CA02 and CA01 stations (Fig. 12 top and middle). The CA01 station was divided by the CA02 station (Fig. 12 bottom).

Our analyses indicate the lack of amplifications on the NS and vertical components for CA03 and CA01 stations with respect to the reference station CA02. In contrast, clear amplifications emerge on the EW component. The SSR between CA03 and CA02 shows amplification peaks between 2 and 4 Hz on the EW horizontal component, with amplitudes that reach the mean value of 3. The SSR between CA01 and CA02 shows amplifications between 5-8 Hz on the EW component. Finally, the SSR between (CA03) and (CA01) shows amplification at 3 Hz on the EW component.

Figure 13 shows the waveforms of three earthquakes of magnitude 4.1, 3.5 and 2.5 recorded by the three stations of the network. The 2-4 Hz band-pass filtered waveforms (red) overlap the original waveforms (black). The CA03 station amplitudes are larger than those of the other two stations in the frequency band where spectral ratios are amplified. There is also a clear effect on the signal duration which is extended by a few tens of seconds.

These considerations are corroborated by the analysis of the ground motion (Fig. 14) and HVSR (Fig. 15) related to an earthquake of Ml 2.4 on 17 July 2009 recorded during the seismic noise measurements at CVS5 and CVS6 stations (Fig. 5).

CVS5 was located in the uppermost portion of the ridge while CVS6 on the western flank. The three-components records of CVS5 (red curves in Fig. 14a) and CVS6 (black curves in Fig. 14a) show that the waveforms for the NS and VT components are comparable. On the contrary, the CVS5 EW component has a persistent and larger amplitude. Figure 14b shows the spectra of the velocity waveforms shown in Figure 16a. It is possible to note that CVS5 EW shows larger amplitude levels starting from about 2 Hz. On the other hand, the spectra peaks at about 1.5 Hz of both the stations are comparable.

The HVSR analysis also show remarkable amplification differences at CVS5 and CVS6 stations (Fig. 15). Indeed, the CVS5 HVSR shows a polarization of the horizontal amplification around 75°N oriented (Fig. 15 top) in the whole frequency range (i.e., 1-10 Hz); moreover, the HVSR shows remarkable amplifications at about 4 Hz. Conversely, CVS6 HVSR shows moderate amplifications in different directions. Finally, the 1.5 Hz HVSR peak is oriented towards 75°N and 115°N for CVS5 and CVS6, respectively.

These results confirm the outcomes of the analyses of the seismic events recorded by the temporary seismic network (CA03, CA02 and CA01 stations).

5. Comparison with synthetic spectra

In order to further test the reliability of CA02 as a reference station, that is, the absence of significant site amplifications, we compared the ground motion recorded at such station during the two above mentioned

events (Ml 3.5 and Ml 4.1) with simulated signals. The standard point-source stochastic approach proposed by Boore (1983; 2003) was adopted to generate synthetic seismograms. We used the classical omega-square model to describe the earthquake source and the path effect is parameterized by simple functions that account for geometrical spreading and anelastic attenuation. The aim is to asses the expected ground motion at CS considering a simple theoretical model of the earthquake source and wave propagation processes.

The source-to-site distances are 50 and 46 km for the larger and smaller event, respectively. In order to account for the frequency-dependent attenuation of the ground motion along the travel path we used the results of Bindi et al. (2009) in terms of quality factor and geometrical spreading. The authors inverted the records from 12 events of the L'Aquila sequence recorded by the Italian strong-motion network (RAN, Rete Accelerometrica Nazionale), in order to separate the contribution of path, source and site effects to the total ground motion. The input parameters adopted in this study are reported in Table 3.

A key parameter of the model, often affected by large uncertainties, is the stress parameter ($\Delta\sigma$), controlling the high-frequency energy of the radiated spectra. We performed the simulations considering three values of $\Delta\sigma$ (i.e., 50, 100 and 150 bar), selected to roughly include all the values obtained by Bindi et al. (2009) for their dataset. Finally, the high-frequency decay parameters (κ) was set to 0.015s which is a reasonable value for hard-rock sites (Margaris and Boore 1998; Bindi et al. 2004).

Figure 16 shows the comparison between recorded and simulated acceleration Fourier Amplitude Spectra (FAS). The simulated FAS represents the root mean square (RMS) of the spectra obtained for 40 realizations of the stochastic process. The increasing amplitudes of the RMS spectra correspond to increasing $\Delta\sigma$ values.

Overall, the simulated spectra are in good agreement with the observed ones at station CA02, for both events. A better fit seems to be provided using a $\Delta\sigma$=100 bar for the larger event and $\Delta\sigma$=150 bar for the smaller one. A slight underestimation of the observed spectra is visible around 2 Hz for both events, possibly related to small site amplification effects at the reference station. When considering CA03 station, only few tens of meters distant, the larger amplitude of the observed spectra compared to the simulated ones becomes evident between 2 and 6 Hz. In particular, the simulated FAS (considering the best fit stress parameters) underestimates the observed EW spectra of about a factor 4 at 3 Hz, for both events.

This comparison support the use of CA02 as a reference station since the recorded spectra are well fitted by those simulated with a simple model for a generic hard-rock site.

6. Discussion

The results of ambient seismic noise measurements plus data derived from three temporary seismic stations have shown an evident heterogeneity of the amplifications within the village. In particular, amplifications of the horizontal components have been found along the CS ridge, with local variations of the frequency bands and amplitudes, ranging between 1 and 15 Hz. In the surrounding areas, instead, no ground motion amplification has been detected.

The NHVSR analyses indicate that the largest amplifications of the horizontal components of the ground motion occur at the uppermost portion of the ridge, perpendicularly to its major elongation axis.

The HVSR and SSR, calculated by means of weak motions recordings confirm the amplification detected by NHVSRs, with amplifications between 1 and 7 Hz and amplitudes larger than roughly 3. Moreover, such amplifications produce the increase of the duration of seismic shaking of some tens of seconds.

As for the cause of the ground motion amplification, topographic effect is generally considered as the main factor that influences local site effects along small and narrow mountain ridges (e.g. Géli and Bard 1988; Massa et al. 2010). It must be noted that topographic effects involve the whole relief and is due to the fundamental frequency of resonance of ridges(Faccioli et al. 2002). Furthermore, they are characterised by an increase of the amplification amplitude from the base to the top of the ridge. These two seismological features are clearly visible and definitive in many cases, e.g. in the case of Castelnuovo village, severely damaged by the April 6, 2009 earthquake (Gallipoli et al. 2009). Nevertheless, the marked heterogeneities concerning frequency, amplitude and polarization in the local seismic response of the CS ridge suggest that other causes - analysed below - have to be invoked to better explain at least part of the observed ground motion amplification.

The results of our geological/structural investigations, coupled with quantitative geomechanical analyses of the jointing condition of the rock mass, have shown that the limestone bedrock of the CS ridge is affected by different deformation style between the lowermost and the uppermost sectors.

In detail, our analyses revealed that the lowermost portion of the rock mass is characterised by pervasive deformation, with vertical, narrowly spaced shear planes and closed fractures, related to the main tectonic features that affect the CS area, i.e. the above mentioned westernmost segment of the SVF and transfer faults. This deformation resulted in a limestone bedrock characterised by "very poor" geomechanical properties, as testified by the indexes achieved by quantitative analyses of the rock mass conditions performed at measurement stations CS3, CS4 and CS6 (Table1) .

Conversely, the uppermost portions of the ridge is mainly characterised by rock slabs – i.e. "block-type" deformation – separated by moderately spaced joints and fractures (geomechanical stations CS5 and CS8). Also, differently from the lowermost sectors, the joints sets paralleling the NW-SE trending branch of the SVF are open of up to some tens of centimetres at the very top of the ridge.

This "picture" allows to hypothesise that the heterogeneity of the local seismic response is related to the depicted structural characteristics of the CS ridge. Indeed, despite a low rock quality at the lowermost portions of the rock mass, no significant ground motion amplification has been here identified. On the other hand, ground motion amplifications strongly increase at the uppermost portion of the ridge and displays a NE-SW orientation, i.e. striking perpendicularly to the major axis of the ridge and to the attitude of the open fractures, as the seismic waves determine the oscillation of the different rock slabs perpendicularly to the main attitude of the open fractures (Fig. 17a).

Hence, all the above highlight that where the fractures are not open no amplification (or very low) occurs and no evident correlation with the trend of the structural features is seen (Fig. 17 b,c,d,e). Therefore, the described structural setting, coupled with the morphological characteristics of the relief, that have favoured the spreading of the fractures, can be considered as one of the main factors that contributes to the ground

motion amplification occurring in the uppermost sector of the CS relief.

This interpretation is also confirmed by the data obtained by the temporary seismic network. Indeed, despite the pervasive and intense deformation of the limestone bedrock (as testified by the results obtained at geomechanical station CS1), ground motion amplification has not been detected along the Mt. Urano slopes (i.e. the reference site; station CA02) (Fig. 17e, CS1-CV18), affected by closed joints; conversely, station CA03, installed at the top of the ridge, showed clear evidence of ground motion amplification perpendicular to the trend of the open fractures (Fig.17a, CS5-CVS3).

7. Concluding remarks

The analysis of the intensity distribution related to the April 6, 2009 L'Aquila seismic event (Mw 6.3) revealed that Castelvecchio Subequo (CS) has been affected by an "anomalous", relatively high degree of damage (i.e. Is 7 MCS scale). The anomaly lies in the fact that the village is about 40 km far from the earthquake source and it is nearby other inhabited centres to which considerably lower intensities, i.e. Is 5-6, have been attributed. Moreover, the damage was irregularly distributed within CS, being mainly concentrated in the uppermost portion of the old village.

We performed geophysical investigations, combined with geological/structural and geomechanical field surveys, that revealed the occurrence of site effects at CS.

In particular, ground motion amplification have been identified at the uppermost portion of the ridge where structural and geomechanical analyses revealed that the limestone bedrock is affected by open joints and fractures related to the main structural features that affect the area, i.e. the westernmost fault segment of the SVF and transfer faults linking the SVF and the Middle Aterno Valley Fault. In particular, the trend of ground motion amplification is parallel to the opening direction of the fractures. Conversely, in other portions of the ridge – in particular, along the lowermost sectors – although the bedrock is affected by intense fracturing and the quality of the rock mass is poor, the joints are not opened and no significant ground motion amplification has been seen.

In the whole, these observations suggest that, besides the age and the typology of the buildings, the damage related to the 2009 earthquake at CS can also related to the local geological characteristics of the area and, in particular, to the style of deformation of the limestone rocks of the CS ridge.

Finally, from an applied point of view, the results obtained indicate that the local geological complexities represent an element of fragility of the CS territory that must be taken into thorough account to better plan the actions necessary to reduce the seismic risk.

Acknowledgements

We are grateful to the Municipality of Castelvecchio Subequo, to the association "Gruppo Archeologico Superequano" and to all the people who live in the study area, who often helped us in the field investigations, sometimes also cooking for us. We are particularly grateful to Gianfranco Calcagni, our irreplaceable guide and fine connoisseur of the country matters.

References

Anzidei M, Boschi E, Cannelli V, Devoti R, Esposito A, Galvani A, Melini D, Pietrantonio G, Riguzzi F, Sepe V, Serpelloni E (2009) Coseismic deformation of the destructive April 6, 2009 L'Aquila earthquake (central Italy) from GPS data. Geophys. Res. Lett. 36, L17307. doi:10.1029/2009GL039145

Athanasopoulos G.A., Pelekis P.C., Leonidou E.A. (1999) Effects of surface topography on seismic ground response in Egion (Greece) 15 June 1995 earthquake. Soil Dynamics and Earthquake Engineering, 18:135 149

Atzori S, Hunstad I, Chini M, Salvi S, Tolomei C, Bignami C, Stramondo S, Trasatti E, Antonioli A, Boschi E (2009) Finite fault inversion of DInSAR coseismic displacement of the 2009 L'Aquila earthquake (central Italy). Geophys. Res. Lett. 36, L15305

Bagh S, Chiaraluce L, De Gori P, Moretti M, Govoni A, Chiarabba C, Di Bartolomeo P, Romanelli M (2007) Background seismicity in the Central Apennines of Italy: The Abruzzo region case study. Tectonophysics 444:80-92

Bard, P. Y. (1982) Diffracted waves and displacement fields over twodimensional elevated topographies. Geophys. J. Int. 71:731–760

Bard P. Y., Tucker B. E. (1985) Underground and ridge site effects: A comparison of observation and theory, Bull. Seismol. Soc. Am. 75:905–922

Bindi D, Castro R, Franceschina G, Luzi L, Pacor F (2004) The 1997 - 1998 Umbria - Marche sequence (central Italy): Source, Path and Site effects estimated from strong motion data recorded in the epicentral area. J. Geophys. Res. 109, B04312. doi:10.1029/2003JB002857

Bindi D, Pacor F, Luzi L, Massa M, and Ameri G (2009) The Mw 6.3, 2009 L'Aquila earthquake: source, path and site effects from spectral analysis of strong motion data. Geophysical Journal International, 179: 1573–1579

Boncio P, Lavecchia G, Pace B (2004) Defining a model of 3D seismogenic sources for Seismic Hazard Assessment applications: The case of central Apennines (Italy). J. Seismol. 8:407-425

Boncio P, Pizzi A, Brozzetti F, Pomposo G, Lavecchia G, Di Naccio D, Ferrarini F (2010) Coseismic ground

deformation of the 6 April 2009 L'Aquila earthquake (central Italy, Mw6.3). Geophys. Res. Lett. 37, L06308.

Boore D. M. (1972) A note on the effect of simple topography on seismic SH waves, Bull. Seismol. Soc. Am. 62:275–284

Boore DM (1983) Stochastic simulation of high-frequency ground motion based on seismological models of the radiated spectra. Bull. Seism. Soc. Am. 73:1865–1894

Boore DM (2003) Simulation of ground motion using the stochastic method. Pure Appl. Geophys. 160:635–676

Borcherdt RD (1970) Effects of local geology on ground motion near San Francisco Bay: Bull. Seism. Soc. Am. 60:29-61

Bosi C, Bertini T (1970) La geologia della media valle dell'Aterno. Mem. Soc. Geol. It. 9:719-777

Bouchon M., Barker J. S. (1996) Seismic response of a hill: The example of Tarzana, California. Bull. Seismol. Soc. Am. 86:66–72

Calamita F, Pizzi A, Scisciani V, De Girolamo C, Coltorti M, Pieruccini P, Turco E (2000) Caratterizzazione delle faglie quaternarie nella dorsale appenninica umbro-marchigiana-abruzzese. CNR-Gruppo Nazionale per la Difesa dai Terremoti, Roma

Cavinato GP, De Celles PG (1999) Extensional basins in the tectonically bimodal central Apennines fold-thrust belt, Italy: response to corner flow above a subducting slab in retrograde motion. Geology. 27:955-958

Çelebi, M. (1987) Topographical and geological amplifications determined from strong motion and aftershock records of the 3 March 1985 Chile earthquake. Bull. Seismol. Soc. Am. 77:1147–1167

Chávez-García F., Sánchez L. R., Hatzfeld D. (1996) Topographic site effects and HVSR. A comparison between observation and theory. Bull. Seismol. Soc. Am. 86:1559–1573

Devoti R, Riguzzi F, Cuffaro M, Doglioni C (2008) New GPS constraints on the kinematics of the Apennines subduction. Earth Planet. Sci. Lett. 273:163-174

Emergeo Working Group (2010) Evidence for surface rupture associated with the Mw 6.3 L'Aquila

earthquake sequence of April 2009 (central Italy). Terra Nova 22:43-51

Faccioli E., Vanini M., Frassine L. (2002) “Complex” site effects in earthquake ground motion, including topography. 12th European Conf. on Earthquake Engineering, Barbican Center, London, UK

Falcucci E, Gori S, Moro M, Galadini F, Marzorati S, Ladina C, Piccarreda D, Fredi P (2009) Evidenze di fagliazione normale tardo-olocenica nel settore compreso fra la conca Subequana e la Media Valle dell'Aterno, a sud dell'area epicentrale del terremoto di L'Aquila del 6 Aprile 2009. Implicazioni sismotettoniche. GNGTS 28° Convegno Nazionale, 16-19 Nov., Trieste (Italy)

Falcucci E, Gori S, Moro M, Pisani AR, Melini D, Galadini F, Fredi P (in press) The 2009 L’Aquila earthquake (Italy): what next in the region? Hints from stress diffusion analysis and normal fault activity. Earth and Planetary Science Letters.

Falcucci E, Gori S, Peronace E, Fubelli G, Moro M, Saroli M, Giaccio B, Messina P, Naso G, Scardia G, Sposato A, Voltaggio M, Galli P, Galadini F (2009) The Paganica fault and surface coseismic ruptures caused by the 6 April, 2009, earthquake (L’Aquila, central Italy). Seism. Res. Lett. 80:940-950

Foglio CARG 1:50,000 (2009) Cartografia Geologica Ufficiale. Foglio N. 369, Sulmona

Galadini F, Galli P (2000) Active tectonics in the central Apennines (Italy) – Input data for seismic hazard assessment. Nat. Hazards 22:225-270

Galadini F, Pantosti D, Boncio P, Galli P, Messina P, Montone P, Pizzi A, Salvi S (2009) Il terremoto del 6 aprile e le conoscenze sulle faglie attive dell’Appennino centrale. Progettazione Sismica 3, ISSN 1973-7432

Galli P. and Camassi R (2009) Rapporto sugli effetti del terremoto aquilano del 6 aprile 2009; Dipartimento della Protezione Civile Istituto Nazionale di Geofisica e Vulcanologia QUEST Team, http://emidius.mi.ingv.it/DBMI08/aquilano/query_eq/quest.pdf

Gallipoli MR, Albarello D., Ceddia M., Da domo A., Di Giacomo D., Giocoli A., Lizza C., Mucciarelli M., Picozzi M., Pilz M., Piscitelli S., Romano G., Sogni D., Vignola L. (2009) Misure speditive di geofisica superficiale a supporto della microzonazione in fase di mergenza. GNGTS 28° Convegno Nazionale, 16-19 Nov., Trieste (Italy)

Géli L, Bard PY (1988) The effect of topography on earthquake ground motion: A review and new results, Bull. Seismol. Soc. Am. 78:42–63

Graizer V (2009) Low-velocity zone and topography as a source of site amplification effect on Tarzana Hill, California, Soil Dynam. Earthquake Eng. 29:324–332

Griffiths DW, Bollinger GA (1979) The effect of Appalachian Mountain topography on seismic waves, Bull. Seismol. Soc. Am. 69:1081–1105

Hailemikael S, Lenti L, Martino S, Paciello A, Scarascia Mugnozza G (2010) 2D numerical modelling of observed amplification effects on a carbonate ridge: the Colle di Roio (Italy) case-history. Proc. 14 European Conference on Earthquake Engineering (ECEE) - Ohrid (Macedonia), 30-08/03-09 2010, n°1662, 1-8

Kawase H, Aki K (1990) Topography effect at the critical SV-wave incidence: Possible explanation of damage pattern by the Whittier Narrows, California, earthquake of 1 October 1987, Bull. Seismol. Soc. Am. 80:1–22

Komatitsch D, Vilotte JP (1998) The spectral element method: An efficient tool to simulate the seismic response of 2D and 3D geological structures, Bull. Seismol. Soc. Am. 88:368–392

Konno K, Ohmachi T (1998) Ground-motion characteristics estimated from spectral ratio between horizontal and vertical components of microtremors. Bull. Seism. Soc. Am. 88:228-241

LeBrun B, Hatzfeld D, Bard PY, Bouchon M (1999) Experimental study of the ground motion on a large scale topographic hill at Kitherion (Greece). J. Seismol. 3:1–15

Lermo J, Chavez-Garcia FJ (1993) Are Microtremors Useful in Site Response Evaluation? Bull. Seism. Soc. Am. 84:1350-1364

Margaris BN, Boore DM (1998) Determination of $\Delta\sigma$ and κ_0 from Response Spectra of Large Earthquakes in Greece. Bull. Seism. Soc. Am. 88:170-182

Martino S, Minutolo A, Paciello A, Rovelli A, Scarascia Mugnozza G, Verrubbi V (2006) Seismic microzonation of jointed rock-mass ridges through a combined geomechanical and seismometric approach. Natural Hazards 39:419-449

Massa M, Lovati S, D'Alema E, Ferretti G, Bakavoli M (2010) Experimental approach for estimating seismic amplification effects at the top of a ridge and their implication on ground motion predictions: the case of Narni (Central Italy). Bull. Seism. Soc. Am. in press

McNamara DE, Buland RP (2004) Ambient Noise Levels in the Continental United States. Bull. Seism. Soc. Am. 94, 4:1517-1527

Miccadei E, Barberi R, De Caterini G (1997) Nuovi dati geologici sui depositi quaternari della conca Subequana (Appennino abruzzese). Il Quaternario (Italian Journal of Quaternary Sciences) 10,2:85-488

Nakamura Y (1989) A method for dynamic characteristics estimations of subsurface using microtremors on the ground surface. Quarterly Rept. RTRI Japan, 30:25-33

Nogoshi M, Igarashi T (1971) On the amplitude characteristics of microtremor (part 2). Journal of Seismological Society of Japan 24:26-40 (In Japanese with English abstract)

Paolucci R (2002) Amplification of earthquake ground motion by steep topographic irregularities. Earthquake Eng. Struct. Dynam. 31:1831–1853

Patacca E, Scandone P, Di Luzio E, Cavinato GP, Parotto M (2008) Structural architecture of the central Apennines: Interpretation of the CROP 11 seismic profile from the Adriatic coast to the orographic divide. Tectonics 27, TC3006

Pedersen H (1994) Ground-motion amplitude across ridges, Bull. Seismol. Soc. Am. 84:1786–1800

Pischiutta M, Cultrera G, Caserta A, Luzi L, Rovelli A (2010) Topographic effects on the hill of Nocera Umbra, central Italy. Geophys. J. Int. 2, 182:977-987. doi: 10.1111/j.1365-246X.2010.04654.x

Pondrelli S, Salimbeni S, Ekstrom G, Morelli A, Gasperini P, Vannucci G (2006) The Italian CMT dataset from 1977 to the present. Physics of the Earth and Planetary Interiors 159:286-303

Rossi A, Tertulliani A, Vecchi M (2005) Studio macrosismico del terremoto dell'Aquilano del 24 giugno 1958. Il Quaternario (Italian Journal of Quaternary Sciences) 18:101–112

Rovelli A, Caserta A, Marra F, Ruggiero V (2002) Can seismic waves be trapped inside an inactive fault zone? The case study of Nocera Umbra, central Italy. Bull. Seism. Soc. Am. 92:2217–2232

Sánchez-Sesma FJ (1985). Diffraction of elastic SH waves by wedges. Bull. Seismol. Soc. Am. 75:1435–1446.

Sánchez-Seisma FJ (1990) Elementary solutions for response of a wedgeshaped medium to incident SH and SV waves. Bull. Seismol. Soc. Am. 80:737–742

Sánchez-Sesma FJ, Campillo M (1991) Diffraction of P, SV, and Rayleigh waves by topographical features: A boundary integral formulation. Bull. Seismol. Soc. Am. 81:2234–2253

Sanchez-Sesma F, Herrera I, Aviles J (1982) A boundary method for elastic wave diffraction: application to scattering of SH waves by surface irregularities, Bull. Seism. Soc. Am. 72:473-490

Spudich P, Hellweg M, Lee WH (1996) Directional topographic site response at Tarzana observed in aftershocks of the 1994 Northridge, California, earthquake: Implication for mainshock motion. Bull. Seismol. Soc. Am. 86:193–208

Tertulliani A, Rossi A, Cucci L, Vecchi M (2009) L'Aquila (Central Italy) earthquakes: the predecessors of the April 6, 2009 event. Seismological Research Letters 80,6:972-977

Working Group CPTI (2008) Catalogo Parametrico dei Terremoti Italiani, versione 2008 (CPTI08). INGV, Bologna, Italy. http://emidius.mi.ingv.it/CPTI/ (Last check of the availability: Sept. 2010)

Tables

Table 1 – Geomechanical characterisation of the rock masses (ISRM 1978; Hudsnon and Priest 1979; Hoek and Bray 1981). As for the joint set codes, see text.

Station	Elevation (m a.s.l.)	Geomorphological features	Joint set	Geomechanical features
CS1	478	Bottom of the slope	III	**Types rock mass:** highly fractured-**Spacing:** extremely close (<20 mm) **Opening:** very close-**Filling:** W1-**Jv:** 50-**JRC:** 8-10-**Undulation:** segmented-polished (III)-**RQD:** <25% very poor
CS2	503	top of the hill	II - IV	**Types rock mass:** highly fractured-**Spacing:** extremely close (<20 mm) **Opening:** close- **Filling:** W1-**Jv:** 38-40-**JRC:** 8-10 **Undulation:** segmented-polished (III)-**RQD:** <25% very poor
CS3	495	Md-slope/top of the hill	IV	**Types rock mass:** highly fractured-**Spacing:** extremely close (<20 mm) **Opening:** close-**Filling:** W1-**Jv:** 45-**JRC:** 8-10 **Undulation:** segmented-polished (III)-**RQD:** <25% very poor
CS4	475	Mid-slope	I - IV	**Types rock mass:** highly fractured-**Spacing:** extremely close (<20 mm) **Opening:** partially open-close-**Filling:** W1 and W2-**Jv**: 42-40-**JRC:** 8-10 **Undulation:** segmented-polished (III)-**RQD:** <25% very poor
CS5	483	top of the hill	I - IV	**Types rock mass:** slabs- **Spacing:** moderate (200 to 600 mm) **Opening**: extremely wide-**Jv:**8-5-**JRC:** 2-4-**Undulation:** smooth-flat (VII)-**RQD:** 75-90% good
CS6	470	Bottom of the slope	I - IV	**Types rock mass:** highly fractured-**Spacing:** extremely close (<20 mm) **Opening:** open-partially open- **Filling:** W1 and W2-**Jv:** 47-42-**JRC:** 8-10 **Undulation:** segmented-polished (III)-**RQD:** <25% very poor
CS7	495	Bottom of the slope	II - IV	**Types rock mass:** highly fractured-**Spacing:** extremely close (<20 mm) **Opening:** partially open-close-**Filling:**W1-**Jv:**42-**JRC:** 8-10 **Undulation:** segmented-polished (III)-**RQD:** <25% very poor
CS8	485	top of the hill	I - IV	**Types rock mass:** slabs- **Spacing:** moderate (200 to 600 mm) **Opening:** extremely wide-**Jv:** 7-10-**JRC:** 2-4-**Undulation:** smooth-flat (VII) **RQD:** 75-90% good
CS9	528	top of the hill	I - III	**Types rock mass:** highly fractured-**Spacing:** extremely

				close (<20 mm) **Opening:** partially open-close-**Filling:**W1-**Jv:** 40-**JRC:** 8-10 **Undulation:** segmented-polished (III)-**RQD:** <25% very poor
CS10	500	Mid-slope	II - III	**Types rock mass:** highly fractured-**Spacing:** extremely close (<20 mm) **Opening:** partially open-close-(III)- **Filling:** W1-**Jv:** 38-42-**JRC:** 8-10- **Undulation:** segmented-smooth (III) **RQD:** <25% very poor

Table 2 – Description of the measurement sites. Code = site name; Amplif = presence of amplification; Amplitude: maximum amplitude of HVSR related to Main Direction; Freq = frequency of HVSR maximum amplitude; Main Direction = degree from the North of the clear direction of amplification; Noise = noise measurement; Earthquake = number of the earthquakes recorded at the site; Ground = type of ground

Code	Amplif	Amplitude	Freq	Main Direction	Noise	Earthquake	Ground
CA01	Yes					295	rock
CA02	No					234	rock
CA03	Yes					308	rock
CVS1	Yes	4.37	6.49	35	x		rock
CVS2	Yes	5.95	3.98	60	x		rock
CVS3	Yes	11.38	6.19	75	x		paved
CVS4	Yes	3.81	1.69	145	x		rock
CVS5	Yes	5.61	3.88	75	x	1	paved
CVS6	Yes	4.58	21.54	85	x	1	paved
CVS7	Yes	2.94	1.30	65	x		asphalt
CVS8	No				x		asphalt
CVS9	No				x		rock
CV16	Yes	4.85	5.35	35	x		rock
CV17	No				x		rock
CV18	No				x		rock
CV21	No				x		asphalt
CV26	No				x		rock
CV29	Yes	3.89	4.00	140	x		soil
CV30	No				x		rock
CV31	Yes	4.43	3.13	55	x		rock
CV40	Yes	3.93	3.50	95	x		rock
CV72	No				x		soil
CV83	Yes	7.16	3.87	70	x		paved
CV84	Yes	15.77	5.42	70	x		rock
CV85	Yes	4.71	3.85	95	x		rock

Table 3 – Parameters used in the simulations

parameter	**value**
shear-wave velocity (V_s) *	3.2 km/s
Density (ρ) *	2.8 gm/cm^3
geometrical spreading *	1/r
quality factor *	$Q=59f^{0.56}$
κ	0.015s
stress parameter	50 - 100 -150 bar
* *from Bindi et al. 2009*	

Figure captions

Figure 1. a) Intensity (Mercalli-Cancani-Sieberg scale; b) distribution of the 2009 L'Aquila earthquake; b) Seismotectonic framework of the central Apennines (modified after Galadini et al., 2009). Faults: MVEF, Mt. Vettore; NFS, Norcia; LMF, Laga Mts.; UAVFS, upper Aterno Valley; CIFS, Campo Imperatore; CF-OPF, Campo Felice-Ovindoli-Pezza; MAVFS, middle Aterno Valley; SVF, Subequana Valley; MMF, Mt. Morrone; FF, Fucino; MPF, Maiella-Porrara; ACF, Aremogna-Cinquemiglia; USFS, upper Sangro Valley; red rectangle, the area analysed in the present work; c) shaded relief of the Subequana Valley; red rectangle, the area under investigation; fault traces, according to Falcucci et al. in press; d) panoramic view of the Castelvecchio Subequo limestone ridge; partly collapsed edifices at the uppermost portion of the ridge, inset.

Figure 2. Geological scheme and cross-sections of the area of Castelvecchio Subequo; rose diagrams (insets) on which the azimuth and the relative abundance of the structural discontinuities affecting the limestone bedrock are shown. Each diagram plots the measurements performed within 1-to-4 squared metre of bedrock exposure.

Figure 3. Reverse fault planes (black dashed lines), affecting the carbonate bedrock, that are crosscut by extensional shear planes (white dotted lines) – a close-up image is shown in inset.

Figure 4. a) Panoramic view of the southern termination of the Castelvecchio Subequo ridge; b) close-up photograph showing narrowly spaced shear planes and closed fractures affecting the limestone bedrock at the lowermost portion of the ridge, c) close-up image of the uppermost portion of the ridge, where opening mode discontinuities affect the carbonate bedrock; details of the open fractures (indicated by white triangles) detected along the western (d) and eastern (e) flanks of the ridge; white arrows indicate the direction of toppling of the bedrock slabs; f) block diagram showing the main sets of fractures affecting the Castelvecchio Subequo ridge.

Fig. 5 Ambient seismic noise stations (red triangles) and temporary seismic network (blue triangles) in CS and in its hinterland. CS buildings are represented with light green polygons. Background: Carta Tecnica Regionale (1:5000) Regione Abruzzo. CS buildings are represented with light green polygons. Blue numbers are the elevation a.m.s.l.. Green numbers are elevation relative to height contours.

Fig. 6 Examples of measurements location inside CS. CVS4) cellar excavated directly in the rock; CV85) courtyard; CVS5and CV84) squares.

Fig. 7 Panoramic view of the temporary seismic network (red triangles). CA03 is located in the historical part of CS, in the foundation floor of a building (bottom on the left); CA02 is located on the slope of Urano mountain in the natural cave; CA01 is located at the base of the relief in a cellar inside the rock outcrop.

Fig. 8 Summary of results about NHVSR analysis. WF: Western Flank; UPR: Upper Portion of the Ridge; EF: Eastern Flank; SA: Surrounding Areas. Green lines represent the 36 directions from 0° to 175°. Thick blue line represents the amplitudes in the maximum amplification direction. Thin blue lines represent standard deviation of the amplitudes in the maximum amplification direction. Station code, frequency (Freq HV) and azimuth (Az) of maximum amplitude are marked in the title of each NHVSR plot.

Fig. 9 Summary of results about NHVSR analysis. The map shows the polar plot of NHVSR lines at each measurements site (black code). Green polygons: CS buildings. Red lines: geologic faults. Blue numbers: elevation a.m.s.l.. Green numbers: elevation relative to height contours. Polar plot of NHVSR curves: outer black numbers mark degrees from the North; color bar marks the NHVSR amplitudes. Background: Carta Tecnica Regionale (1:5000) Regione Abruzzo.

Fig. 10 Map of the 903 epicentres resulting from earthquakes data set selected on 9 November 2009. Red triangle marks the position of the CS temporary seismic network. Image taken from http://iside.rm.ingv.it

Fig. 11 Summary of results about earthquake HVSR analysis. NS/UP: HVSR between North-South component and the vertical one. EW/UP: HVSR between East-West component and the vertical one. Thick blue line: HVSR geometrical average; thin blue lines: HVSR standard deviation. Black titles: station code, HVSR type, number of seismic events used for HVSR analysis.

Fig. 12 Summary of results about earthquake SSR analysis. EW/EW: SSR between East-West components. NS/NS: SSR between North-South components. UP/UP: SSR between vertical components.Thick blue line: SSR geometrical average; thin blue lines: SSR standard deviation. Black titles: analysed station code on reference station code, SSR type, number of seismic events used for SSR analysis.

Fig. 13 East-West (EW) waveforms of three earthquakes recorded at CA03, CA01, CA02 stations. Black titles: origin time and magnitude of the seismic event. RIDGE: station at the ridge of the relief; BASE: station at the base of the relief; REF: reference station on the slope of the Urano mountain. Black line: original waveform. Red line: band-pass filtered waveform from 2 to 4 Hz.

Fig. 14 Waveforms (a) and Spectra (b) of a earthquake recorded at CVS5 and CVS6 noise measurement stations. Black title in a): origin time and magnitude of the seismic event. Black lines: CVS6 waveforms and spectra. Red lines: CVS5 waveforms and spectra. EW: East-West component; NS: North-South component; UP: vertical component. VEL: velocity.

Fig. 15 HVSR of the earthquake in Fig. 16. Top: HVSR at CVS5 station. Bottom: HVSR at CVS6 station. Black titles on the left: station code, frequency (Freq HV) and azimuth (Az) of maximum HVSR amplitude. Red lines: HVSR 75°N direction. Blue line: HVSR 115°N direction. Polar plot of NHVSR curves: outer black numbers mark degrees from the North; inner black numbers represent the NHVSR frequency (Hz); color bar marks the NHVSR amplitudes.

Fig. 16 Comparison between observed (gray and black lines) and simulated (red lines) acceleration Fourier Amplitude Spectra. The increasing amplitudes of the simulated FAS correspond to increasing $\Delta\sigma$ values (50, 100 and 150 bars). Simulated FAS have been high-pass filtered at 0.3 Hz. The moment magnitude and hypocentral distance used in the simulations are also reported.

Fig. 17 Structural discontinuities vs amplification directions. Left panels: rose diagrams on which the azimuth and the relative abundance of the structural discontinuities affecting the limestone bedrock; each diagram plots the measurements performed within one squared metre of bedrock exposure. Right panels: polar plot of NHVSR curves; outer black numbers mark degrees from the North; color bar marks the NHVSR amplitudes.

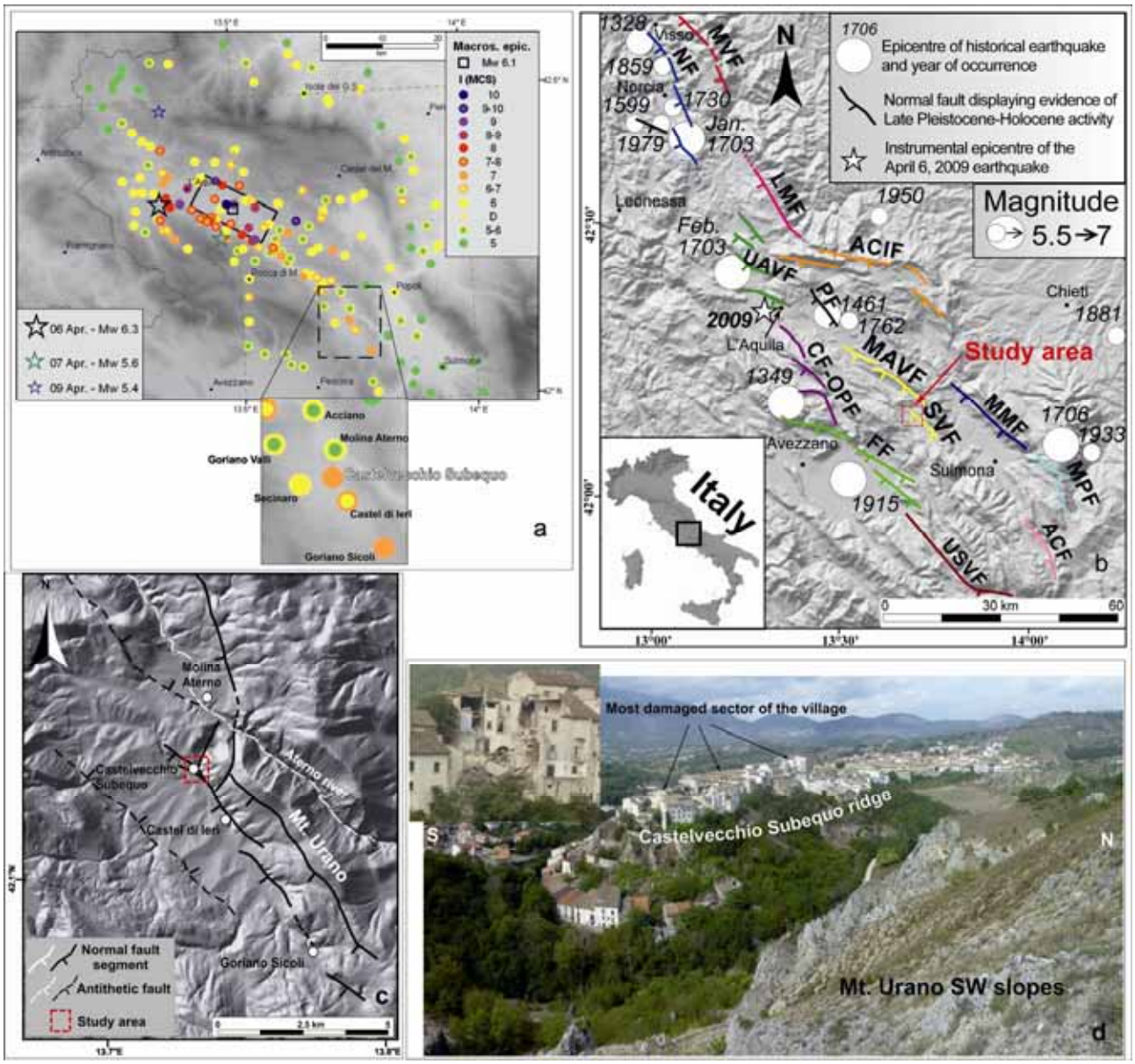
Macros. epic.
Mw 6.1
I (MCS)
10
9-10
9
8-9
8
7-8
7
6-7
6
D
5-6
5
06 Apr. - Mw 6.3
07 Apr. - Mw 5.6
09 Apr. - Mw 5.4
Acciano
Molina Aterno
Goriano Valli
Secinaro
Castel di Ieri
Goriano Sicoli
a
1706
Epicentre of historical earthquake and year of occurrence
Normal fault displaying evidence of Late Pleistocene-Holocene activity
Instrumental epicentre of the April 6, 2009 earthquake
Magnitude
5.5→7
1328
Visso
MVF
NF
1859
Norcia
1599
1730
Jan. 1703
1979
LMF
1950
Leonessa
Feb. 1703
UAVF
ACIF
PF
1461
1762
2009
L'Aquila
1349
CF-OPF
MAVF
Study area
SVF
MMF
1706
1933
Avezzano
FF
Sulmona
MPF
1915
USVF
ACF
Chieti
1881
Italy
b
0
30 km
60
13°00'
13°30'
14°00'
42°30'
42°00'
N
Molina Aterno
Castelvecchio Subequo
Aterno river
Castel di Ieri
Mt. Urano
Goriano Sicoli
Normal fault segment
Antithetic fault
Study area
c
Most damaged sector of the village
Castelvecchio Subequo ridge
S
N
Mt. Urano SW slopes
d

Figure 1

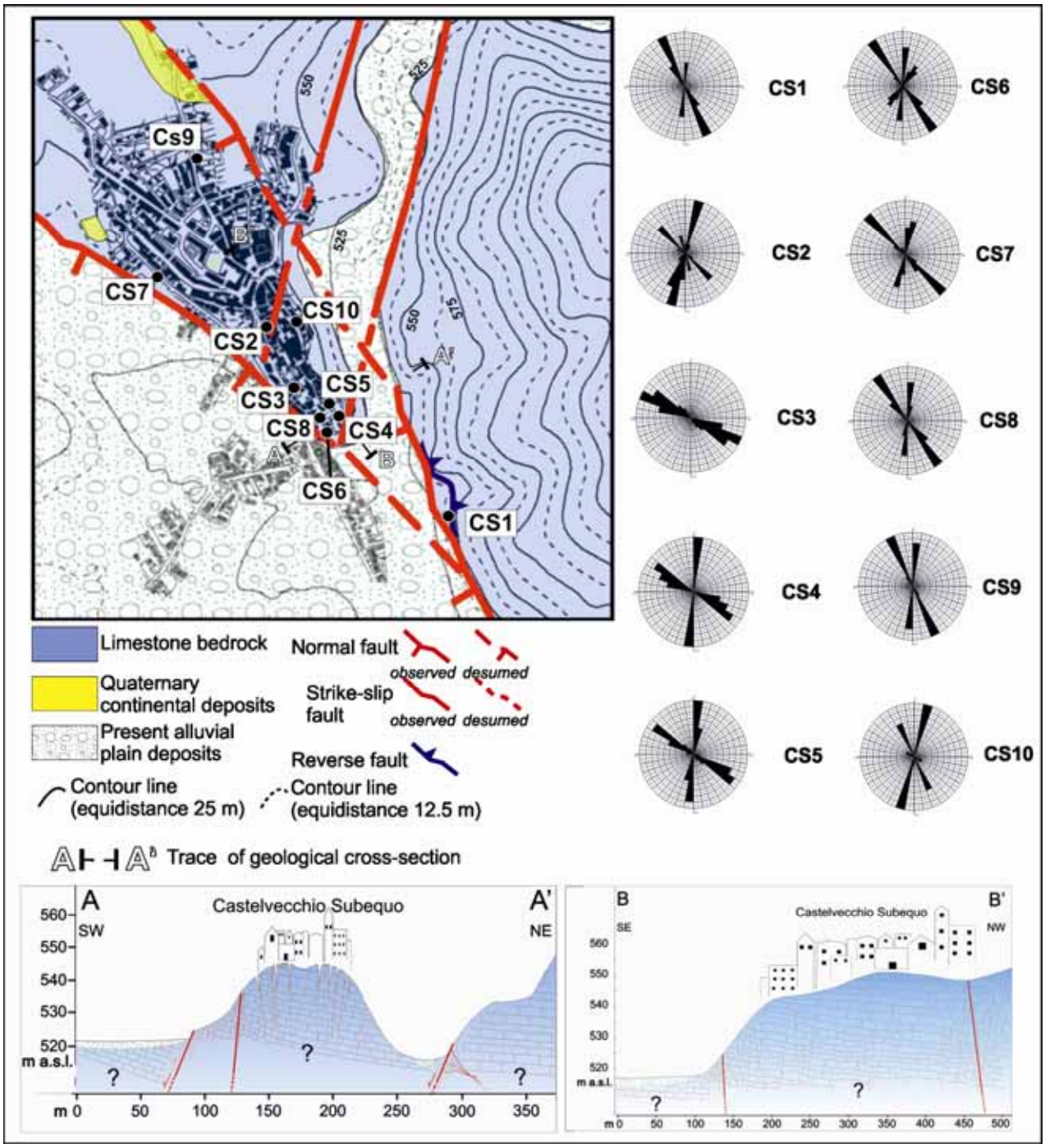
Cs9
CS7
CS10
CS2
CS3
CS5
CS8
CS4
CS6
CS1
A
A'
B
B'
550
525
575
CS1
CS6
CS2
CS7
CS3
CS8
CS4
CS9
CS5
CS10
Limestone bedrock
Quaternary continental deposits
Present alluvial plain deposits
Contour line (equidistance 25 m)
Normal fault
observed
desumed
Strike-slip fault
observed
desumed
Reverse fault
Contour line (equidistance 12.5 m)
Trace of geological cross-section
A
SW
Castelvecchio Subequo
A'
NE
560
550
540
530
520
m a.s.l.
m 0
50
100
150
200
250
300
350
B
SE
Castelvecchio Subequo
B'
NW
560
550
540
530
520
m a.s.l.
m 0
50
100
150
200
250
300
350
400
450
500

Figure 2

Figure 3

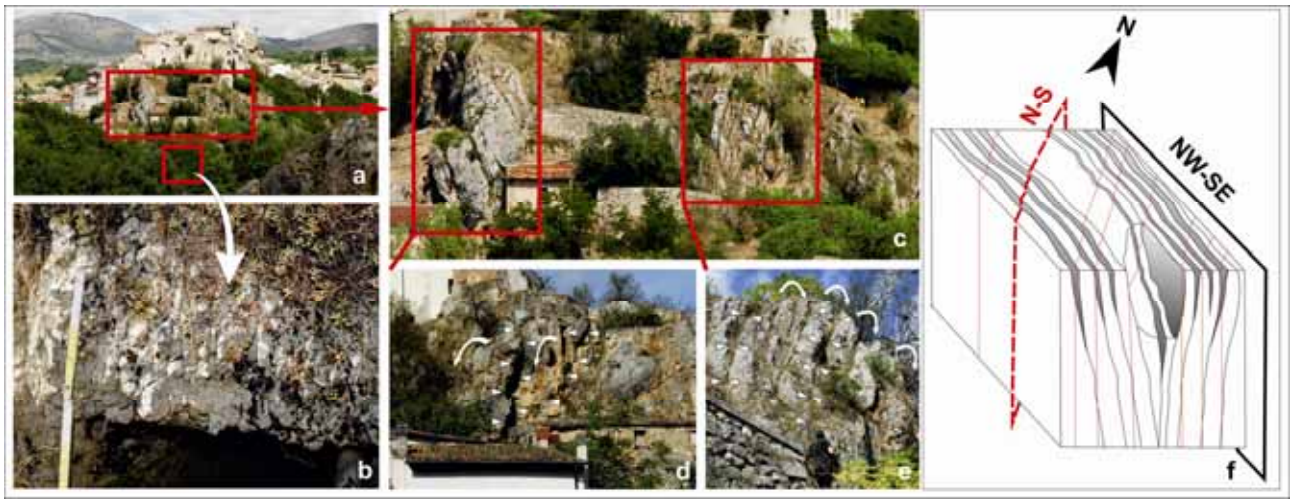

Figure 4

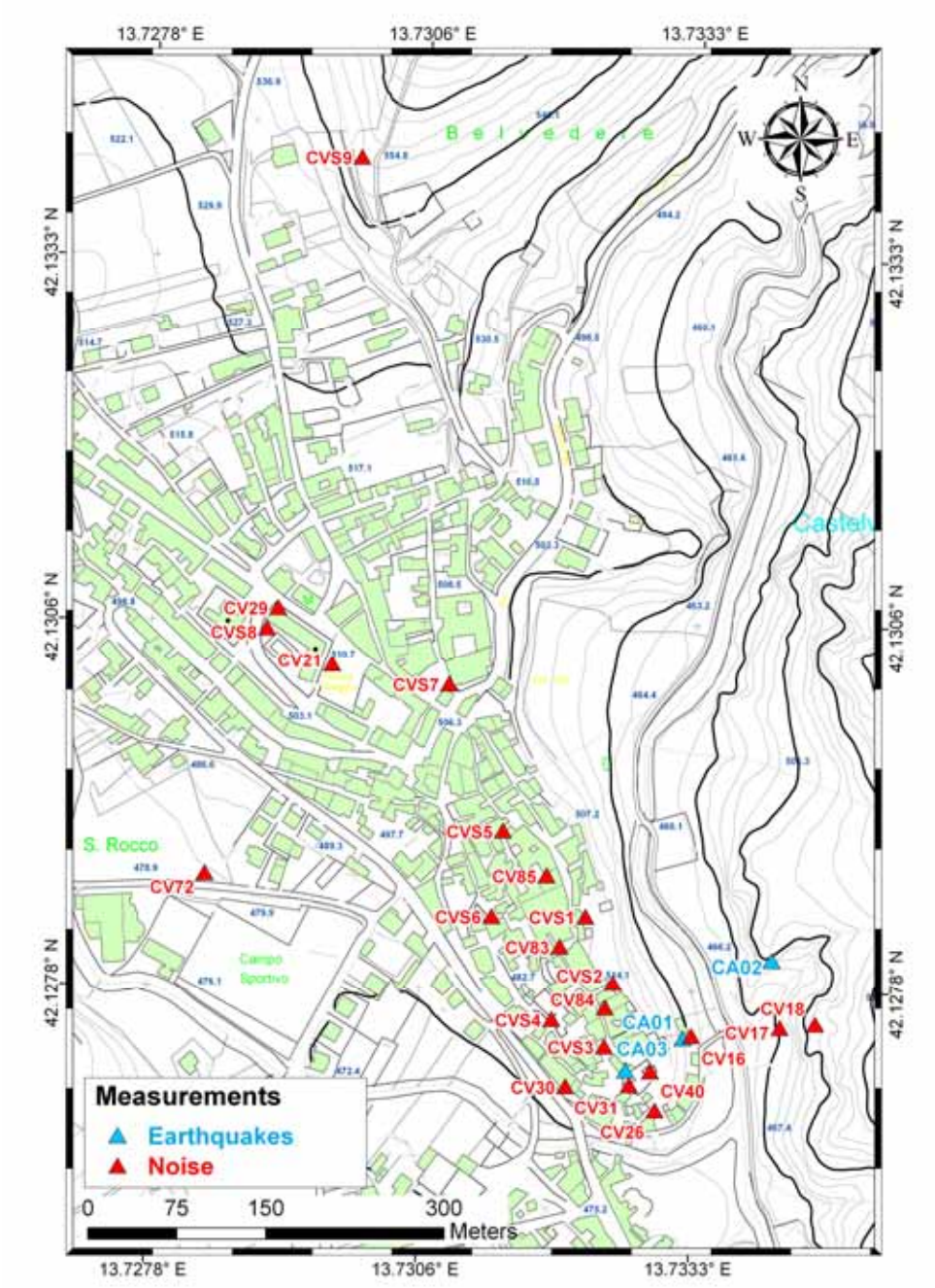
13.7278° E
13.7306° E
13.7333° E
42.1333° N
42.1306° N
42.1278° N
N
W
E
S
Belvedere
S. Rocco
Campo Sportivo
CVS9
CV29
CVS8
CV21
CVS7
CVS5
CV85
CV72
CVS6
CVS1
CV83
CVS2
CV84
CVS4
CVS3
CA01
CA03
CA02
CV18
CV17
CV16
CV30
CV40
CV31
CV26
Measurements
Earthquakes
Noise
0
75
150
300
Meters

Figure 5

Figure 6

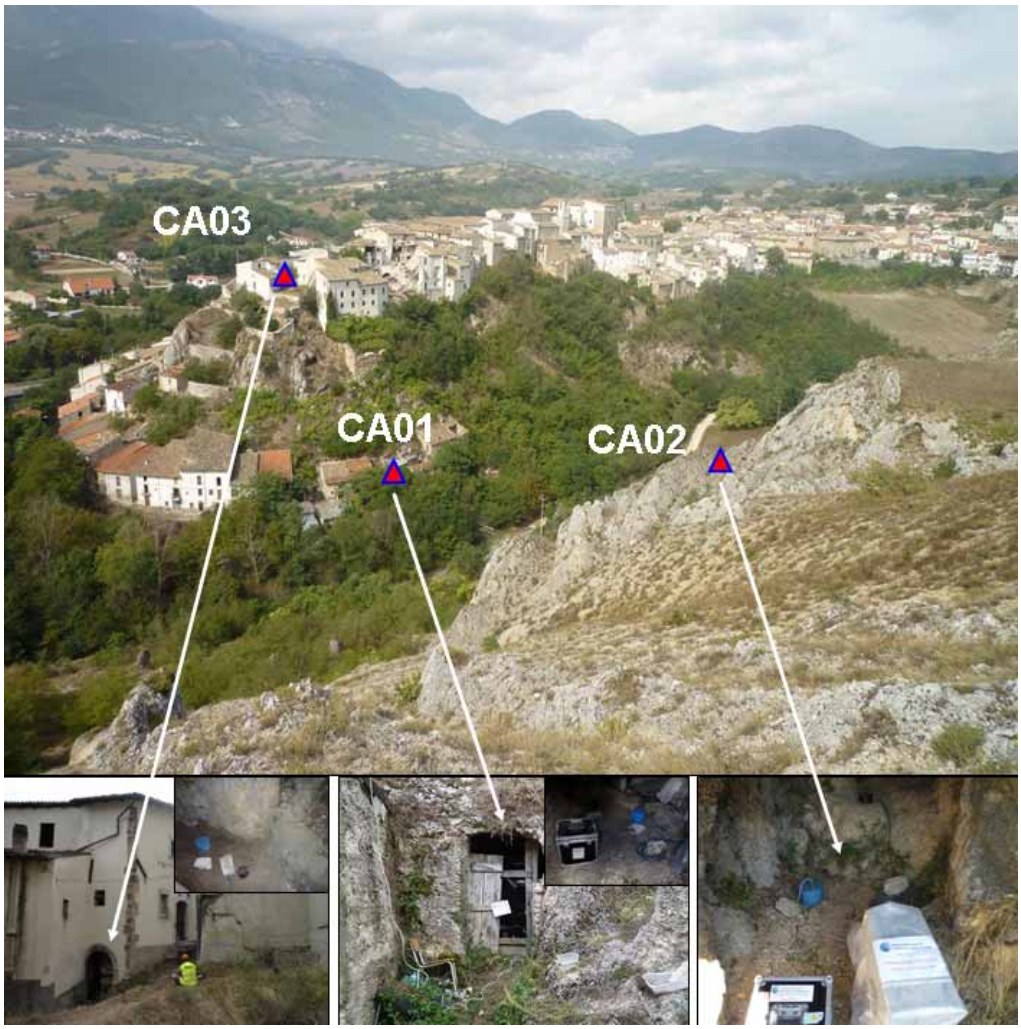

Figure 7

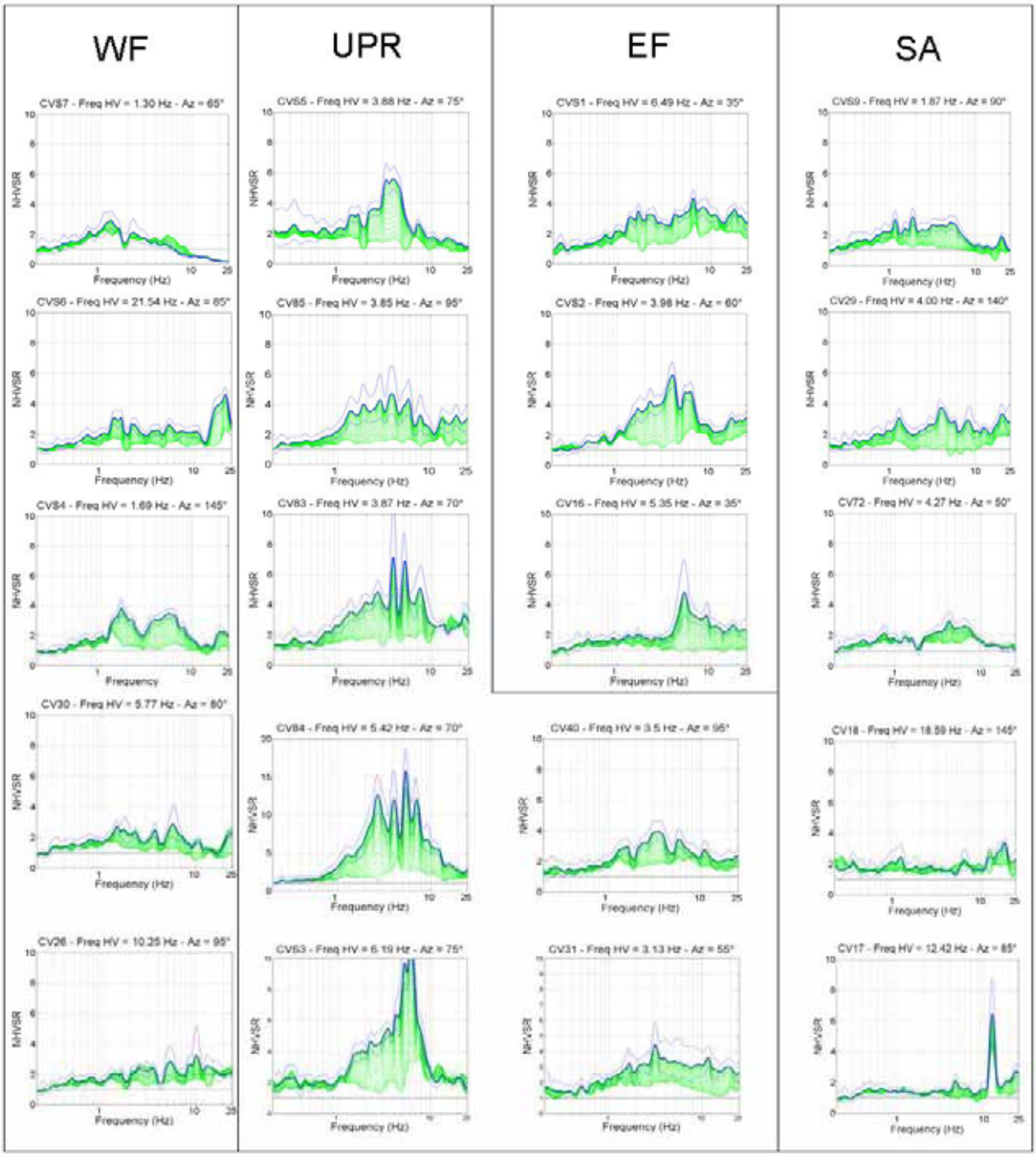
WF
UPR
EF
SA
CVS7 - Freq HV = 1.30 Hz - Az = 65°
CVS5 - Freq HV = 3.88 Hz - Az = 75°
CVS1 - Freq HV = 6.49 Hz - Az = 35°
CV59 - Freq HV = 1.87 Hz - Az = 90°
CVS6 - Freq HV = 21.54 Hz - Az = 85°
CV85 - Freq HV = 3.85 Hz - Az = 95°
CVS2 - Freq HV = 3.98 Hz - Az = 60°
CV29 - Freq HV = 4.00 Hz - Az = 140°
CVS4 - Freq HV = 1.69 Hz - Az = 145°
CV83 - Freq HV = 3.87 Hz - Az = 70°
CV16 - Freq HV = 5.35 Hz - Az = 35°
CV72 - Freq HV = 4.27 Hz - Az = 50°
CV30 - Freq HV = 5.77 Hz - Az = 80°
CV84 - Freq HV = 5.42 Hz - Az = 70°
CV40 - Freq HV = 3.5 Hz - Az = 95°
CV18 - Freq HV = 18.59 Hz - Az = 145°
CV26 - Freq HV = 10.25 Hz - Az = 95°
CV53 - Freq HV = 6.19 Hz - Az = 75°
CV31 - Freq HV = 3.13 Hz - Az = 55°
CV17 - Freq HV = 12.42 Hz - Az = 85°
Frequency (Hz)

Figure 8

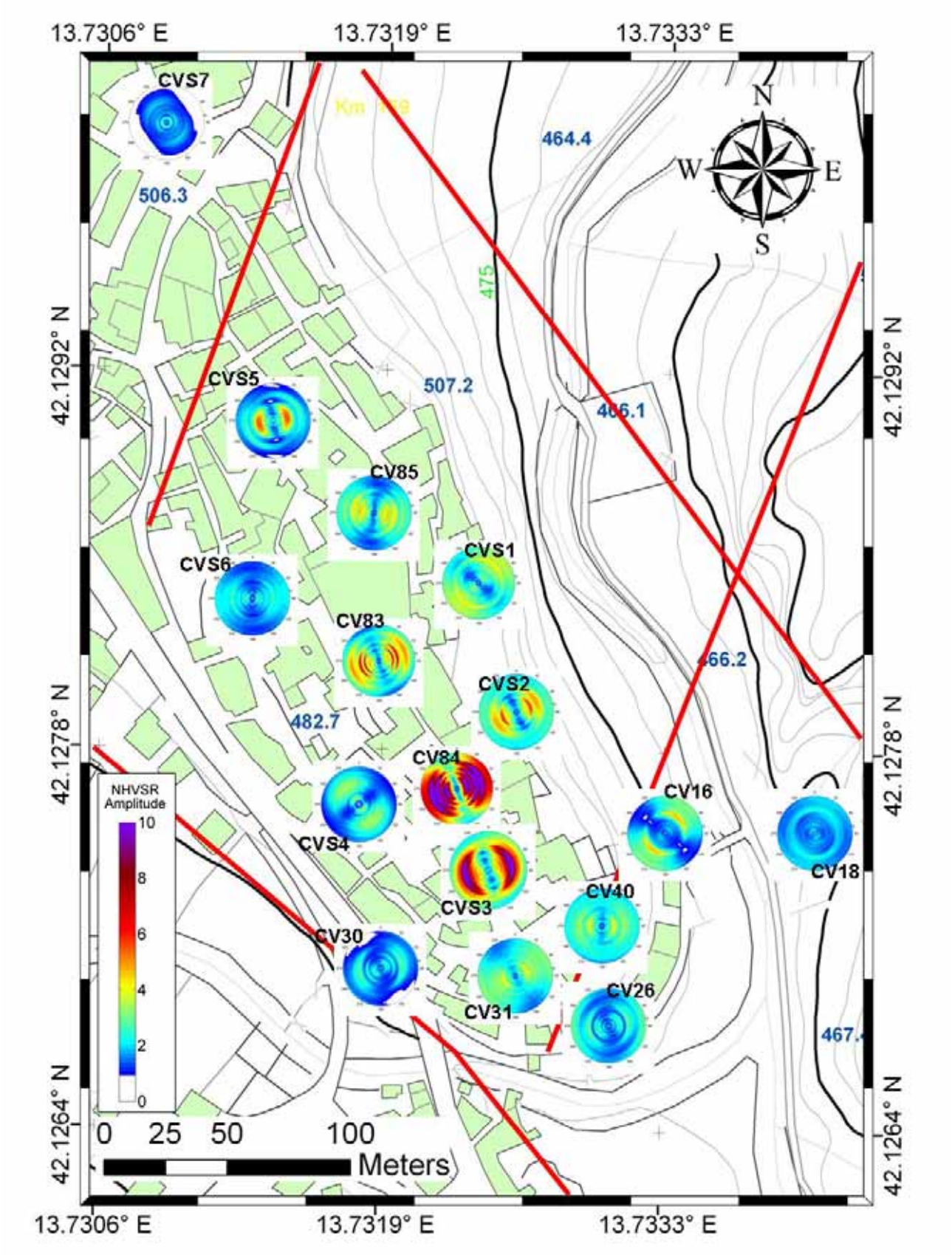
13.7306° E
13.7319° E
13.7333° E
42.1292° N
42.1278° N
42.1264° N
CVS7
CVS5
CVS6
CVS1
CVS2
CVS4
CVS3
CV85
CV83
CV84
CV30
CV31
CV40
CV26
CV16
CV18
506.3
464.4
507.2
466.1
482.7
475
N
W
E
S
NHVSR Amplitude
10
8
6
4
2
0
0 25 50 100
Meters

Figure 9

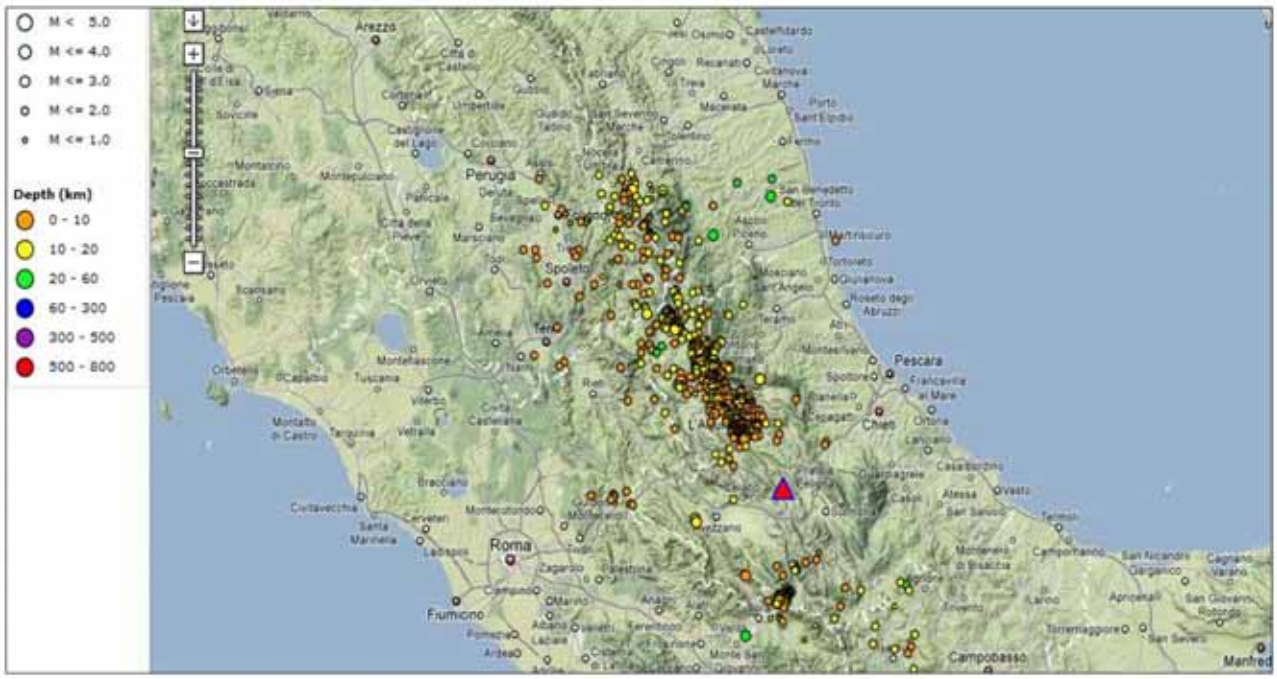
M < 5.0
M <= 4.0
M <= 3.0
M <= 2.0
M <= 1.0
Depth (km)
0 - 10
10 - 20
20 - 60
60 - 300
300 - 500
500 - 800
Arezzo
Perugia
Spoleto
Pescara
Roma
Fiumicino
Campobasso

Figure 10

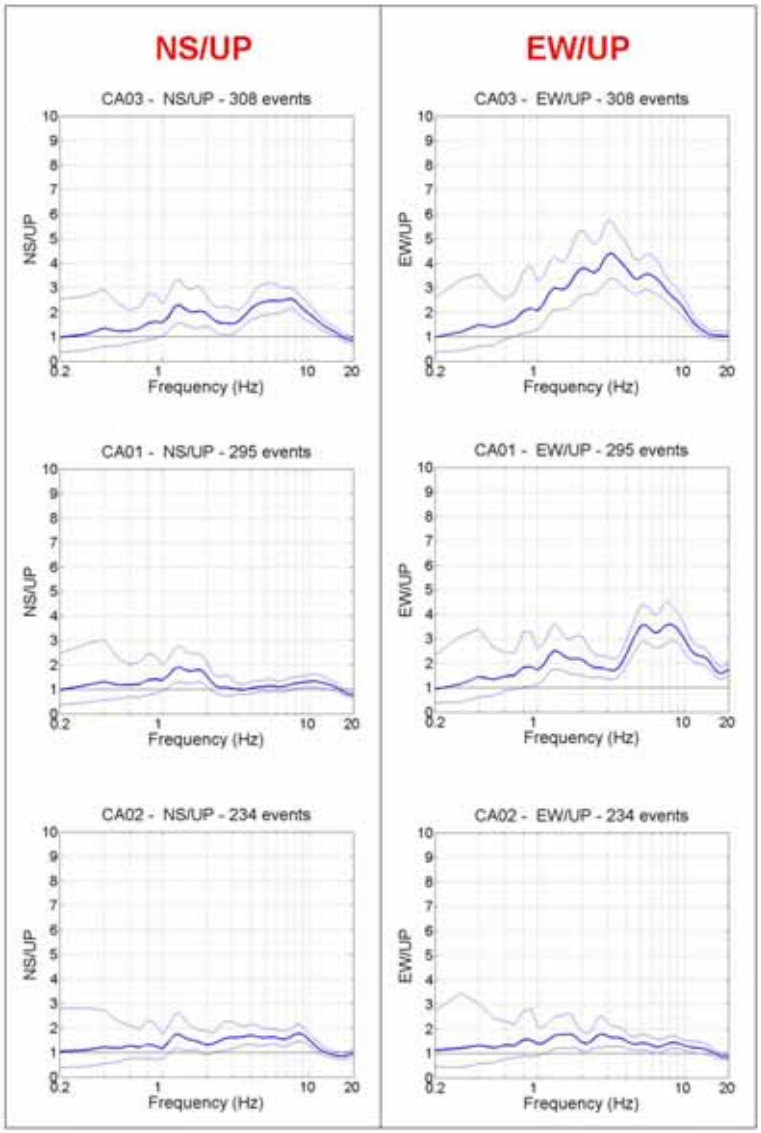
NS/UP
EW/UP
CA03 - NS/UP - 308 events
CA03 - EW/UP - 308 events
CA01 - NS/UP - 295 events
CA01 - EW/UP - 295 events
CA02 - NS/UP - 234 events
CA02 - EW/UP - 234 events
NS/UP
EW/UP
Frequency (Hz)
0.2
1
10
20

Figure 11

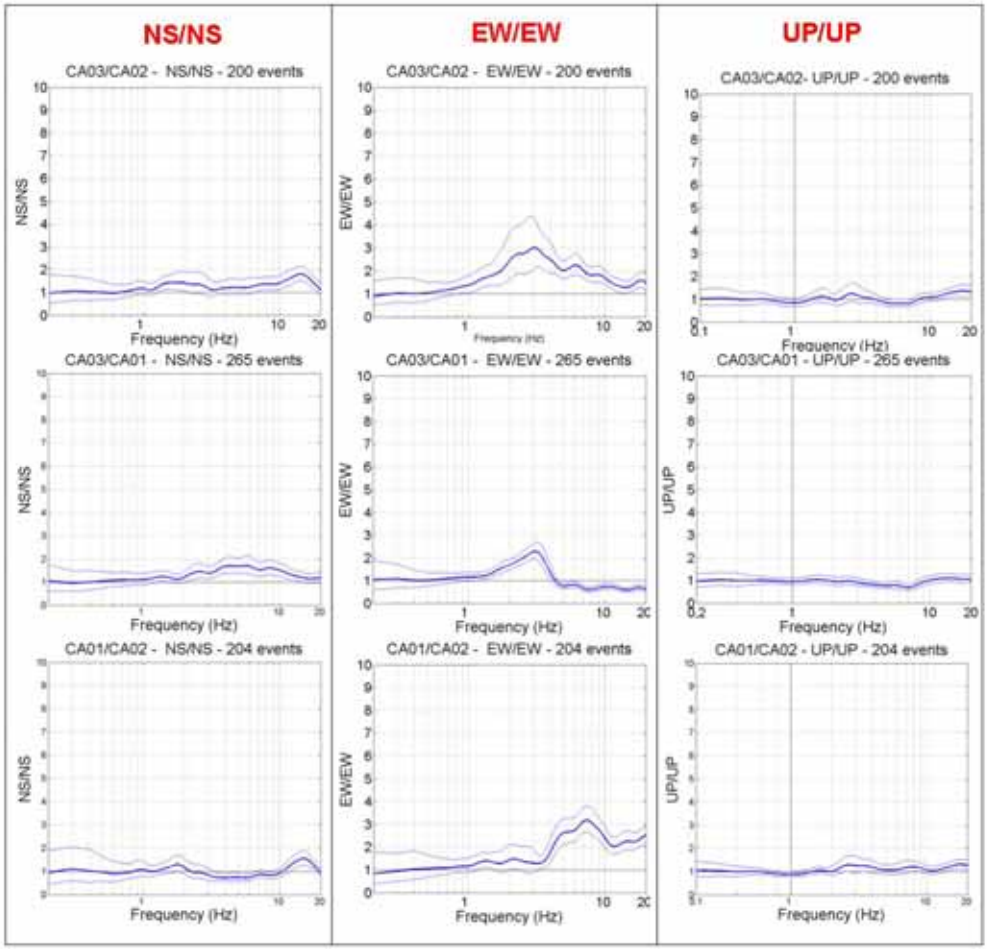
NS/NS
EW/EW
UP/UP
CA03/CA02 - NS/NS - 200 events
CA03/CA02 - EW/EW - 200 events
CA03/CA02- UP/UP - 200 events
CA03/CA01 - NS/NS - 265 events
CA03/CA01 - EW/EW - 265 events
CA03/CA01 - UP/UP - 265 events
CA01/CA02 - NS/NS - 204 events
CA01/CA02 - EW/EW - 204 events
CA01/CA02 - UP/UP - 204 events
NS/NS
EW/EW
UP/UP
Frequency (Hz)

Figure 12

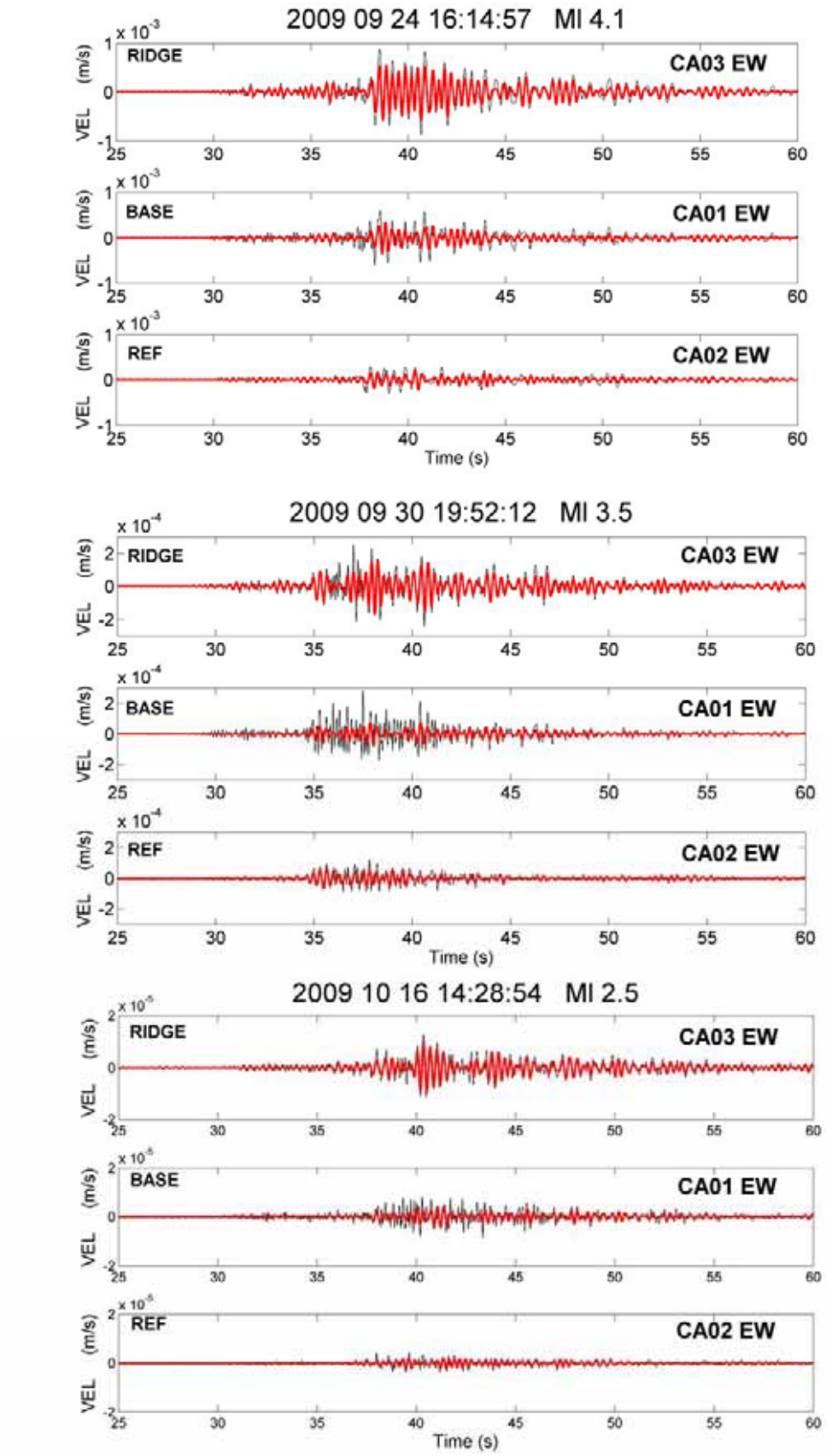
2009 09 24 16:14:57 MI 4.1
RIDGE
CA03 EW
BASE
CA01 EW
REF
CA02 EW
VEL (m/s)
Time (s)
2009 09 30 19:52:12 MI 3.5
RIDGE
CA03 EW
BASE
CA01 EW
REF
CA02 EW
VEL (m/s)
Time (s)
2009 10 16 14:28:54 MI 2.5
RIDGE
CA03 EW
BASE
CA01 EW
REF
CA02 EW
VEL (m/s)
Time (s)

Figure 13

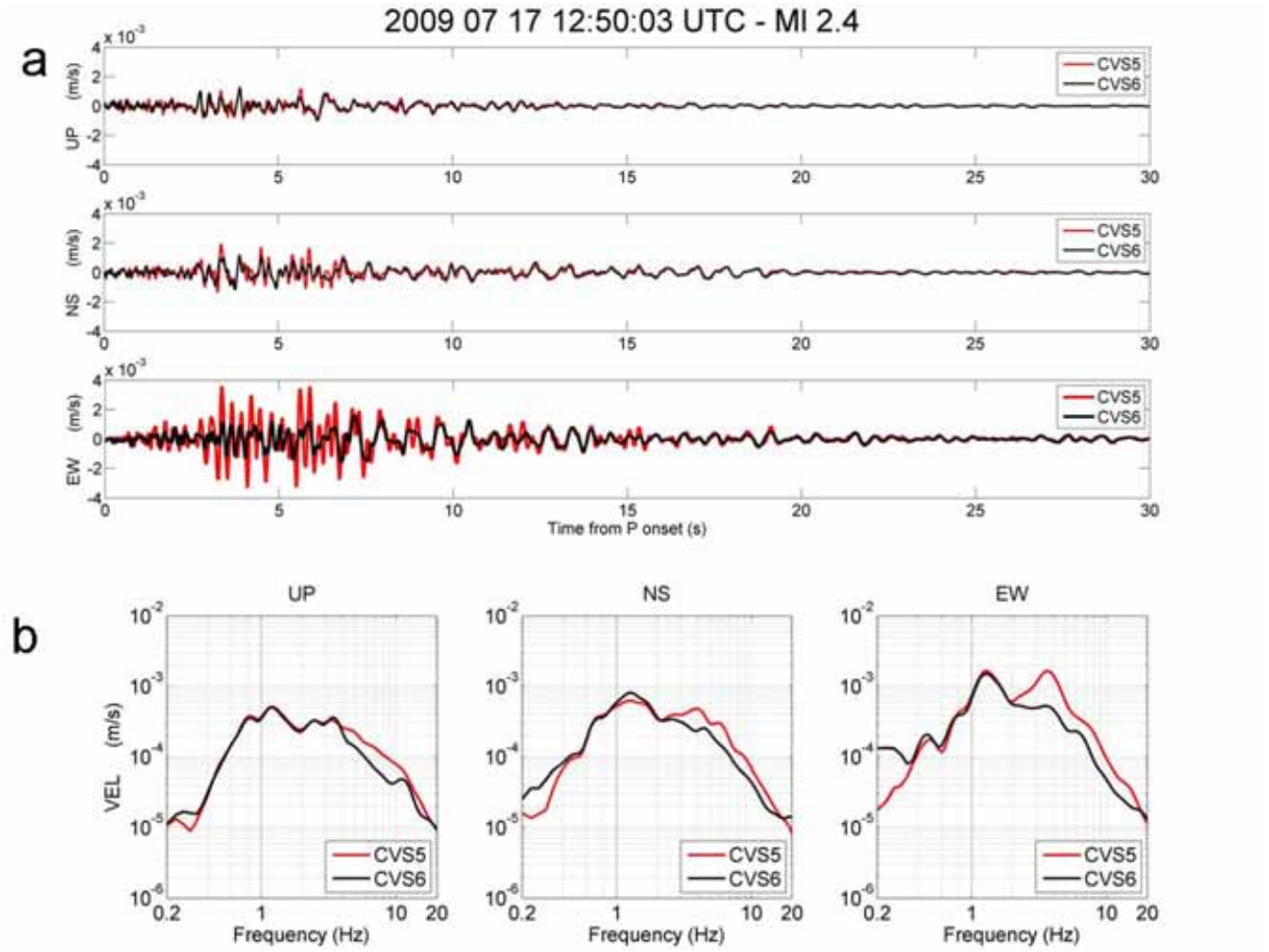
2009 07 17 12:50:03 UTC - MI 2.4
a
b
UP
NS
EW
(m/s)
VEL
CVS5
CVS6
Time from P onset (s)
Frequency (Hz)

Figure 14

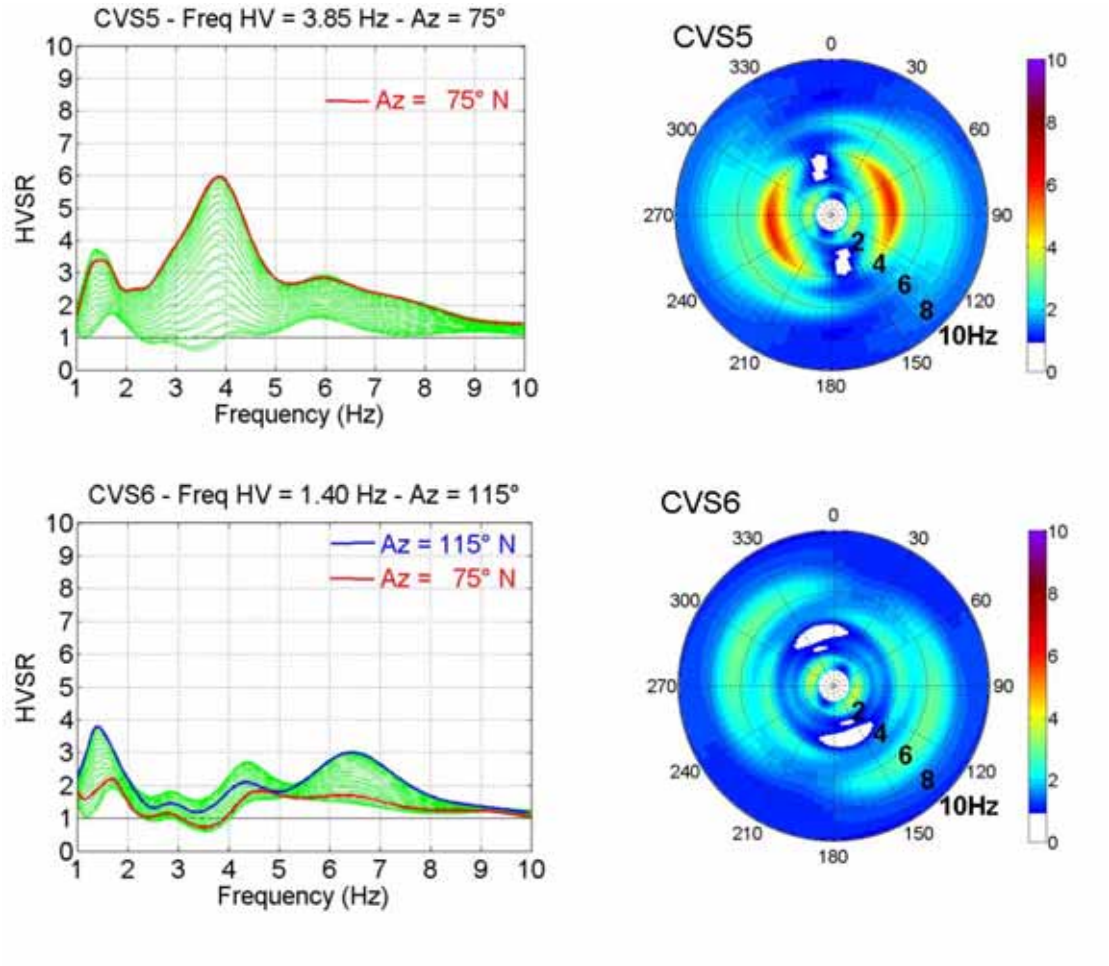
CVS5 - Freq HV = 3.85 Hz - Az = 75°
Az = 75° N
HVSR
Frequency (Hz)
CVS5
10Hz
CVS6 - Freq HV = 1.40 Hz - Az = 115°
Az = 115° N
Az = 75° N
HVSR
Frequency (Hz)
CVS6
10Hz

Figure 15

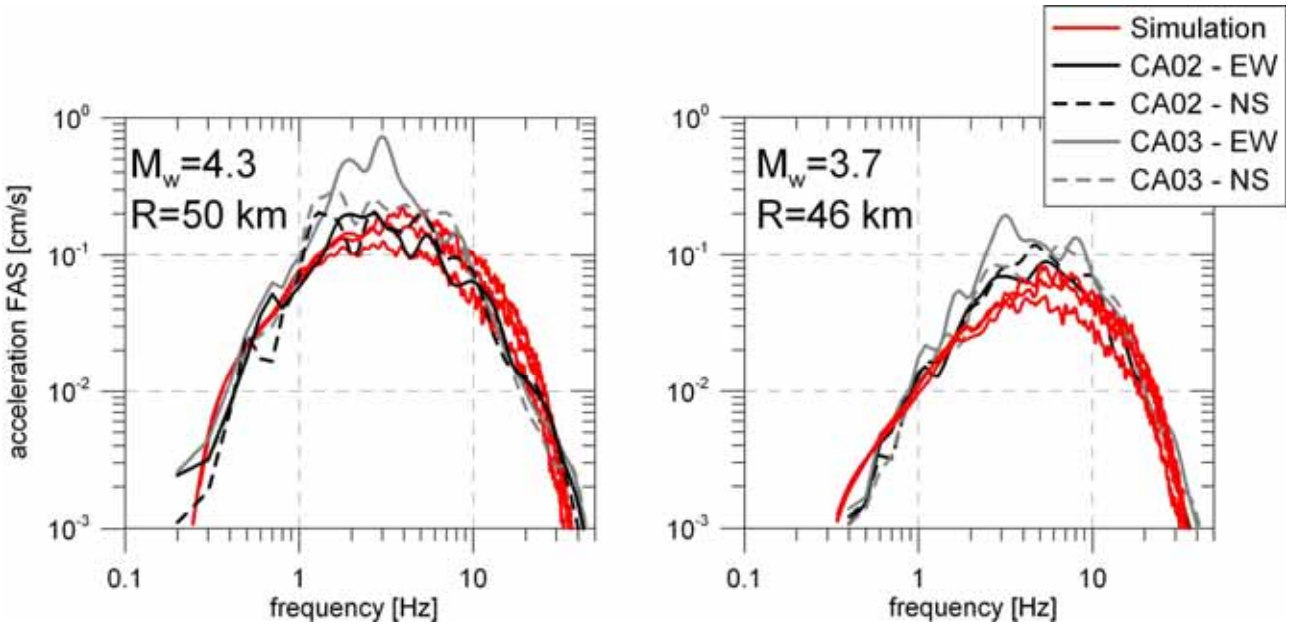
Simulation
CA02 - EW
CA02 - NS
CA03 - EW
CA03 - NS
M_w=4.3
R=50 km
M_w=3.7
R=46 km
acceleration FAS [cm/s]
frequency [Hz]
frequency [Hz]

Figure 16

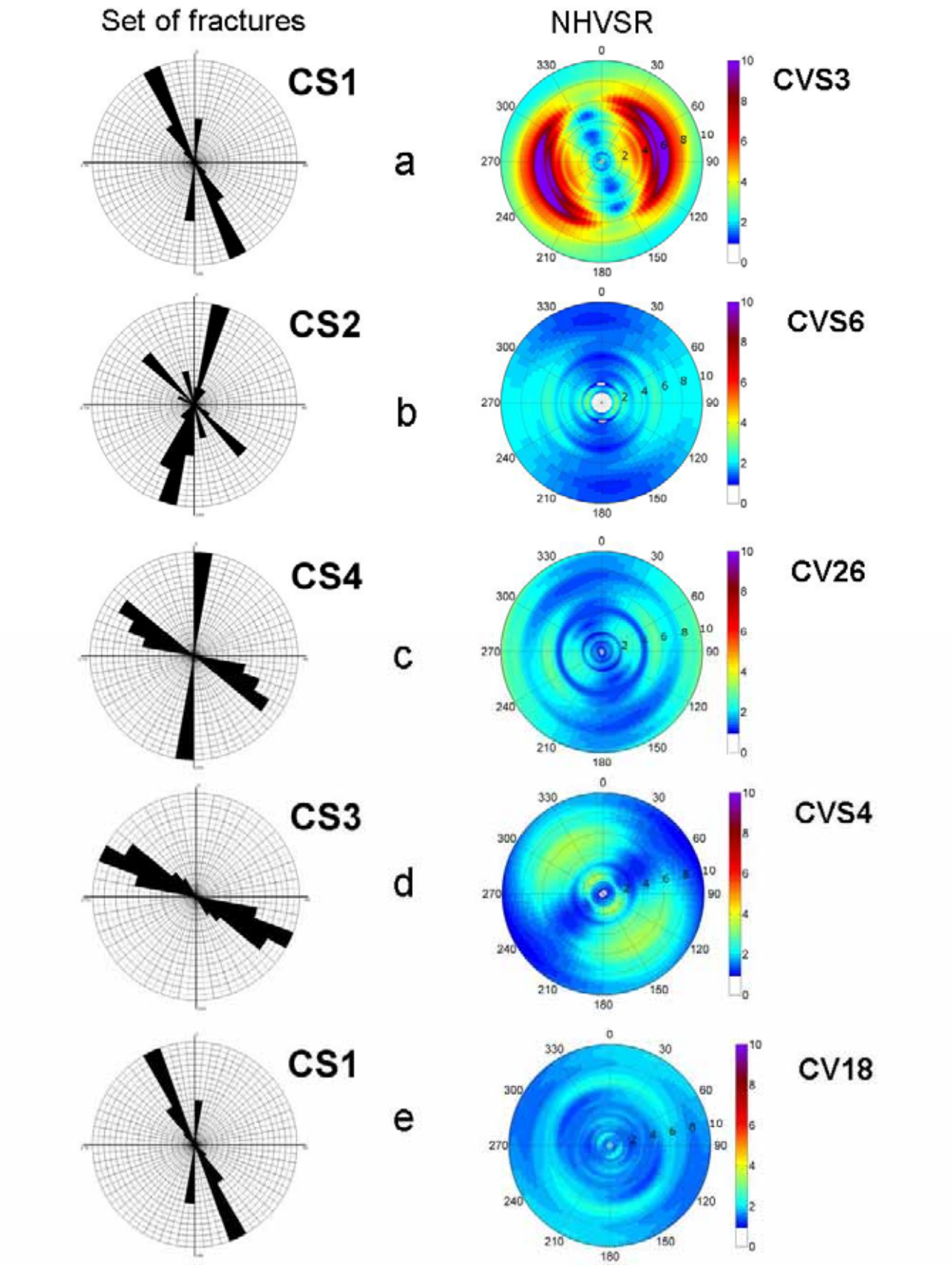
Set of fractures
NHVSR
CS1
a
CVS3
CS2
b
CVS6
CS4
c
CV26
CS3
d
CVS4
CS1
e
CV18

Figure 17